Received: 8 March 2018 | Revised: 2 July 2018 | Accepted: 19 July 2018

DOI: 10.1002/hipo.23017

WILEY

RESEARCH ARTICLE

# Stability of medial entorhinal cortex representations over time

Geoffrey W. Diehl[1] | Olivia J. Hon[1] | Stefan Leutgeb[1,2] | Jill K. Leutgeb[1]

[1]Neurobiology Section and Center for Neural Circuits and Behavior, Division of Biological Sciences, University of California, La Jolla, California

[2]Kavli Institute for Brain and Mind, University of California, La Jolla, California

**Correspondence**
Jill K. Leutgeb, University of California, San Diego, 9500 Gilman Drive # 0357, La Jolla CA 92093.
Email: jleutgeb@ucsd.edu

**Funding information**
National Institute of Mental Health, Grant/Award Numbers: MH100349, MH102841; National Institute of Neurological Disorders and Stroke, Grant/Award Numbers: NS084324, NS086947, NS097772; Whitehall Foundation, Grant/Award Number: 20130571

## Abstract

Distinct functional cell types in the medial entorhinal cortex (mEC) have been shown to represent different aspects of experiences. To further characterize mEC cell populations, we examined whether spatial representations of neurons in mEC superficial layers depended on the scale of the environment and changed over extended time periods. Accordingly, mEC cells were recorded while rats repeatedly foraged in a small or a large environment in sessions that were separated by time intervals from minutes to hours. Comparing between large and small environments, we found that the overall precision of grid and non-grid cell spatial maps was higher in smaller environments. When examining the stability of spatial firing patterns over time, differences and similarities were observed across cell types. Within-session stability was higher for grid cells than for non-grid cell populations. Despite differences in baseline stability between cell types, stability levels remained consistent over time between sessions, up to 1 hr. Even for sessions separated by 6 hrs, activity patterns of grid cells and of most non-grid cells lacked any systematic decrease in spatial similarity over time. However, a subset of ~15% of mEC non-grid cells recorded preferentially from layer III exhibited dramatic, time dependent changes in firing patterns across 6 hrs, reminiscent of previous characterizations of the hippocampal CA2 subregion. Collectively, our data suggest that mEC grid cell input to hippocampus in conjunction with many time invariant non-grid cells may aid in stabilizing hippocampal spatial maps, while a subset of time varying non-grid cells could provide complementary temporal information.

**KEYWORDS**

grid cell, memory, place cell, remapping, temporal context

## 1 | INTRODUCTION

The medial entorhinal cortex (mEC) is composed of numerous functional cell types with highly specialized firing patterns that are well suited for supporting computations critical for spatial navigation and spatial memory (Buzsaki and Moser, 2013; Hartley et al., 2014). Subpopulations of entorhinal neurons represent heading direction, speed, and the position of the animal in space (Fyhn et al., 2004; Kropff et al., 2015; Sargolini et al., 2006), with those cells that are specialized for spatial coding often being further subdivided into grid cells, border cells, and irregular spatial cells (Diehl et al., 2017; Hafting et al., 2005; Savelli et al., 2008; Solstad et al., 2008). In line with a role of mEC providing critical input downstream to hippocampus, subsets of each of these functional classes have been reported to project directly to the hippocampus (Zhang et al., 2013).

Input from spatially selective mEC cells are widely hypothesized to give rise to the highly precise place fields observed in hippocampus, with a wide range of models proposing how such a computation could occur (Blair et al., 2008; Cheng and Frank, 2011; de Almeida et al., 2009; Fuhs and Touretzky, 2006; O'Keefe and Burgess, 1996; Rolls et al., 2006; Solstad et al., 2006). Yet, experimental studies indicate that place coding in hippocampus is at least partially retained after removal or inactivation of mEC (Brun et al., 2008; Hales et al., 2014; Miao et al., 2015; Ormond and McNaughton, 2015; Robinson et al., 2017; Rueckemann et al., 2016; Schlesiger et al., 2015), suggesting that other inputs to hippocampus can compensate for loss of a spatially precise mEC signal. In contrast, mEC projections were found to be critical for CA1 hippocampal map stability (Hales et al., 2014; Schlesiger et al., 2015), indicating that mEC neural circuits may instead be particularly important for providing the hippocampus

  

with a rigid and stable spatial representation. However, the stability of the mEC spatial code over time has not been systematically tested.

While the stability of mEC representations over time is not known, it has recently been established that some of the main hippocampal projection targets of mEC cells show place cell firing patterns that vary over time, even when all key aspects of the experience, such as the spatial environment and the behavioral task, are highly familiar and held constant (Lu et al., 2015; Mankin et al., 2015; Mankin et al., 2012; Rubin et al., 2015; Ziv et al., 2013). In particular, the dissimilarity of neuronal coding over time is pronounced in CA2, where place cell representations of an environment are already dissimilar over intervals of minutes. In contrast, the spatial coding of hippocampal CA3 cells exhibits very limited change, even over periods as long as 30 hrs (Lu et al., 2015; Mankin et al., 2012). The co-occurence of stable and drifting population codes has been proposed to constitute a potential mechanism for decoding how long ago a particular event occurred (Estes, 1955; Howard and Kahana, 2002), and such temporal coding is thought to constitute a critical component of episodic memory representations (Tulving, 1972). In support of these mechanisms being implemented across mammalian species, drifting network representations have also been observed in the medial temporal lobe of humans (Ezzyat and Davachi, 2014; Hsieh et al., 2014; Jenkins and Ranganath, 2016; Manning et al., 2011; Nielson et al., 2015) and have been shown to relate to behavioral performance or subjective evaluations in temporal encoding tasks (Ezzyat and Davachi, 2014; Hsieh et al., 2014; Jenkins and Ranganath, 2016).

Although it is now well established that hippocampal CA1 and CA2 place cell representations gradually change over time, the neuronal circuit and cellular mechanisms that generate such a drifting code have not been identified. While CA3 projects to both CA1 and CA2 (Dudek et al., 2016; van Strien et al., 2009), its highly stable representations makes CA3 an unlikely candidate to provide a drifting signal. One possibility is therefore that the rapid change over time observed within the CA2 region is generated de novo locally, perhaps due to the unique anatomical, cellular, and physiological properties of CA2 cells (Dudek et al., 2016; Jones and McHugh, 2011). A stable signal from CA3 and a drifting signal from CA2 could then combine to give rise to the intermediate stability that has been reported for CA1 (Mankin et al., 2015). Alternatively, extrahippocampal areas, such as the entorhinal cortex, could pass along an either stable or drifting code to one or more hippocampal subregions. Owing to the highly spatial nature of cellular firing within mEC and its strong projections to all hippocampal CA regions, we investigated the stability of mEC firing patterns over extended time periods. To test the stability of mEC spatial representations over extended time, we recorded the activity patterns of the same mEC cell populations while rats explored the same environment at the same location in space over multiple sessions. The temporal intervals between sessions ranged from 5 min to 6 hrs. Grid, border, and irregular cell types were classified within each session and for each functional mEC cell type the stability of the spatial representation was examined across sessions.

## 2 | MATERIALS AND METHODS

### 2.1 | Subjects and surgery

Experimental procedures were performed as approved by the Institutional Animal Care and Use Committee at the University of California, San Diego and according to National Institutes of Health and institutional guidelines. Data were recorded from eight male Long Evans rats (300–400 g) that were housed individually and maintained on a 12-h light/dark schedule with lights off at 7:00 a.m. Data from three rats (45 out of 313 cells) have been previously reported in a different study (Diehl et al., 2017) and were reanalyzed here. Prior to behavioral testing rats were implanted with a "hyperdrive" recording device consisting of 14 independently movable tetrodes. For drive implantation, rats were anesthetized with isofluorane (1.5–2.5% in $O_2$) and given buprenorphine (0.02 mg/kg, S.C.) as an analgesic. After opening a skull window and removing dura, the hyperdrive was implanted above the dorsal mEC 0.5–1.0 mm anterior to the transverse sinus and 4.6–5.2 mm lateral to the midline. Tetrodes were constructed from 17 μm platinum-iridium (90/10%) wire and were plated with a 1.5% platinum solution to lower impedances to 125–325 kΩ at 1 kHz prior to surgery.

### 2.2 | Behavioral procedures

After one week of recovery from surgery, rats were food restricted to 85% of free feeding weight and were trained to forage for randomly scattered cereal crumbs in open field enclosures (80 cm by 80 cm square, 100 cm diameter circle, 120 cm by 120 cm square). Each open field had a single polarizing cue card (20 or 25 cm wide) placed on an internal wall. Environments were always centered in the same location within the room, the position of the cue card was kept constant, and the recording system, experimenter, and other external room cues were readily visible to the rats.

All rats were trained in blocks of four 10-min foraging sessions. Two blocks of four 10-min sessions were conducted each day separated by 6 hrs as described previously (Mankin et al., 2015; Mankin et al., 2012). Training always occurred at the same time of day with the first session starting between 8:00 a.m. and 10:00 a.m. and the second session starting between 2:00 p.m. and 4:00 p.m. Start times varied between rats, but a given rat always ran the morning sessions at the same time and the afternoon sessions 6-hr later. All recording blocks were flanked by 20-min sleep periods and rats were given 5 min between sessions to rest in a pot away from the foraging enclosure. Between sessions the floor of the open field was cleaned with water. Single unit recordings in mEC began when the environments were highly familiar (at least 7 days of prior training) to not confound instability over time with responses to novelty. Behavioral procedures while recording mEC units were identical to training procedures and continued until cells could no longer be recorded.

For three rats, training and recording sessions were performed in the two smaller boxes (80 cm by 80 cm square enclosure and 100 cm diameter circular enclosure) (Diehl et al., 2017). Within each block of four sessions, two of the sessions were in the square environment and two were in the circular environment, with the two shapes

presented in a pseudorandom order. The current analysis focused on the stability of maps, therefore all comparisons were made between sessions of identical shape. For the remaining five rats training and recording sessions were performed in the 120 cm square box with all four recording sessions of each block conducted in the same enclosure.

## 2.3 | Electophysiological recordings

Following surgery, tetrodes were gradually advanced toward the superficial layers of mEC with one tetrode remaining in cortex to serve as a reference. A second tetrode was rapidly advanced through the brain to identify the beginning and end of mEC based on local field potential (LFP) signatures. The remaining 12 recording tetrodes were advanced 25 to 160 μm per day through mEC to record single unit activity. When large amplitude units were observed, tetrodes were not advanced in an effort to record the same cell population multiple times over the course of successive recording sessions, sometimes across multiple days. Advancement of tetrodes and recordings were performed blind to any functional properties of recorded cells ensuring an unbiased sampling of the mEC population. Recordings and advancement of tetrodes continued until LFP criteria indicated that each tetrode had been advanced to Layer 1.

For recording single units and LFP, hyperdrives were connected through a multichannel, head-mounted preamplifier to a digital Neuralynx recording system. Unit activity was amplified and band-pass filtered between 0.6 kHz and 6 kHz. Spike waveforms above a trigger threshold (35–55 μV) were time-stamped and digitized at 32 kHz for 1 ms. Continuous LFP was recorded from each tetrode, filtered between 0.1 Hz and 900 Hz, and sampled at 2000 Hz. Position data of a red and a green LED located on either side of the head-mounted preamplifier were tracked at 30 Hz by a video camera mounted above the experimental area to determine the rat's *x*-*y* position and head-direction.

Spike sorting was manually performed offline using a customized version of MClust (Redish, A.D. MClust. http://redishlab.neuroscience.umn.edu/MClust/MClust.html) (Mankin et al., 2012). Sleep periods before and after behavioral sessions were used to ensure stability of recorded cells. The identity of individual cells was tracked across recording sessions by applying identical cluster bounds across sessions to compare the location of clusters in multidimensional cluster space as has previously been described (Mankin et al., 2015; Mankin et al., 2012). Clusters whose location in cluster space did not change across recording sessions were identified as originating from the same cell. Spiking autocorrelation was occasionally used as a secondary metric for confirming cluster identity across sessions, but importantly no other firing properties, such as spatial firing pattern, head direction firing, or theta modulation, were used to evaluate cells across sessions. Only clusters that had well-separated boundaries were included in the analysis. To quantify the quality of analyzed clusters, we calculated the isolation distance of all recorded cells (Schmitzer-Torbert et al., 2005). While we did not exclude data based on isolation distance, others have set minimum isolation distances of 5 or 10 (Newman and Hasselmo, 2014; Perez-Escobar et al., 2016). Of those clusters that we accepted for analysis, 99.5% had isolation distances of at least 10. Putative interneurons were identified and removed from the data set based on an average firing rate above 7.5 Hz. Note that this threshold is higher than typically used in the hippocampus because many principal cells in entorhinal cortex fire at intermediate rates.

## 2.4 | Histological analysis

At the completion of all experiments, rats were given an overdose of sodium pentobarbital and were perfused transcardially with saline and 4% formaldehyde. Brains were extracted and post fixed for 24 hrs before being transferred to a 30% sucrose solution and allowed to sink. Sagittal sections (40 μm) were cut on a freezing microtome and sections through the right mEC were mounted on slides and stained with cresyl violet. Tetrode trajectories through mEC were determined by 3D reconstruction of the sectioned tissue. Based on records of the systematic movement of tetrodes through the brain and the trajectory information, complemented by records of LFP profiles, tetrode locations on each recording day were assigned to either the deep or superficial layers of mEC. Cells recorded from the superficial layers were further localized to putative recordings from Layer 2 or Layer 3. Any recordings from the deep mEC layers or from the presubiculum or parasubiculum were removed from the data set.

## 2.5 | Rate maps and functional firing properties

Rate maps were constructed by summing the total number of spikes that occurred in each location bin (5 cm × 5 cm), dividing by the total amount of time that the rat occupied the bin, and smoothing with a 5 × 5 bin Gaussian filter with a standard deviation of approximately 1 bin (Diehl et al., 2017):

[0.0025 0.0125 0.0200 0.0125 0.0025;
0.0125 0.0625 0.1000 0.0625 0.0125;
0.0200 0.1000 0.1600 0.1000 0.0200;
0.0125 0.0625 0.1000 0.0625 0.0125;
0.0025 0.0125 0.0200 0.0125 0.0025]

Bins that were never within a distance of less than 2.5 cm from the tracked path or with total occupancy of less than 150 ms were regarded as unvisited and were not included in the rate map. To control for possible influences of stationary episodes, periods below a minimum running speed of 2 cm/s were excluded from all calculations.

To identify grid cells, we evaluated the degree of six-fold rotational symmetry in each cell's spatial auto-correlation by calculating a grid score and comparing it to a surrogate shuffled distribution produced by time shifting spike times with respect to an animal's trajectory as described previously (Diehl et al., 2017). For each cell, we calculated rate maps as above but based on a bin size of 2.5 cm. To then generate the spatial auto-correlation matrix, we calculated the Pearson's correlation between the firing rates of bins at corresponding locations between the rate map and itself. One map was then shifted in the *x* and *y* dimensions and the correlation was taken at all *x*-*y* offsets to produce the auto-correlation matrix. From this matrix, an annulus that contained the first hexagon of peaks around the center,

but excluded the central peak, was extracted. The average correlation value of bins in the annulus was then taken at each angle from the center (i.e., along a "ray"). These values were rotated in 30° steps and correlated to the un-rotated average values. If sixfold symmetry exists, the correlations at 30, 90, and 150° are expected to be low while the correlations at 60 and 120° are expected to be high. A cell's grid score was thus taken as the difference between the average of the latter and the average of the former sets of correlation values. Grid scores were then compared to the 95th percentile of a shuffled distribution of grid scores generated for each individual cell in each session (i.e., chance value), and grid cells were positively identified as those cells for which the majority of sessions had a grid score that exceeded the chance value.

Firing field boundaries for grid cells were calculated as previously described (Diehl et al., 2017) using a reference map across all recordings of the given cell. For recordings from the shape-change paradigm, only the area common to the two shapes (80 × 80 cm) was used to build the reference map. Field bounds were defined on the reference map by building contours iteratively outwards until a threshold value of 0.3 times the peak rate was reached. The minimum peak rate to identify a field was 2 Hz, with a minimum field size of 250 $cm^2$. For cells with multiple fields, contours were calculated simultaneously for all fields, and the edge of each field was defined as the contour at which the threshold value was reached or where two fields met, whichever came first.

To identify border cells, we calculated a border score for each rate map (Solstad et al., 2008). We identified firing fields for each cell in each session as described above using a minimum firing rate of 2 Hz, a threshold value of 0.3 times the peak field rate, and a minimum field size of 250 $cm^2$. The maximal extent of a single field along any wall was taken as $C_M$, the mean firing distance to the nearest wall was taken as $d_m$, and border score was calculated as: $b = \frac{C_M - d_m}{C_M + d_m}$, and ranged from −1 for cells with central firing to 1 for cells with firing aligned to walls. Any rate map in which a firing field could not be identified was not assigned a border score. As for grid cells, border scores were compared to the 95th percentile of a shuffled distribution of border scores generated for each individual cell in each session, and border cells were identified as those cells for which the majority of sessions had a border score that exceeded the chance value. For data recorded from our small environment we identified only four border cells. Due to the low cell number in the small environment, this cell type was only analyzed for the large environment.

To quantify spatial firing of cells we calculated a spatial information score (SI) and a within session correlation (WSC) as described previously. SI per spike was calculated as: $SI = \sum_i P_i \frac{R_i}{R} \log_2 \frac{R_i}{R}$, where $i$ indexes the spatial bins, $P_i$ is the probability of occupancy in each bin, $R_i$ is the mean firing rate in each bin, and $R$ is the mean firing rate across the spatial map (Skaggs et al., 1993). WSC was calculated for each cell in each session by splitting the 10-min recording into the first and second half. Rate maps were calculated for both 5-min periods and a Pearson's correlation was taken between the two (Diehl et al., 2017). As for grid scores, chance level SI and WSC were calculated for each cell in each session by shuffling spike times.

Head Direction (HD) modulation was calculated as the mean resultant length (MRL) of the polar plot generated by comparing cell spiking to angular direction of the animal's head. Using angular bins with one degree resolution, the number of spikes was divided by the amount of time spent at each bin.

Running speed modulation (speed score) was calculated for each cell as the Pearson's correlation between the instantaneous running speed and the instantaneous firing rate (Kropff et al., 2015). Instantaneous running speed was calculated for each camera frame by passing trajectory data through a Kalman filter. Instantaneous firing rate was calculated across all frames in a session by summing the number of spikes that occurred between subsequent frames, dividing by the time between frames, and smoothing with a 250-ms wide Gaussian filter with a standard deviation of 90-ms. Periods below an instantaneous running speed of 2 cm/s and in the top 5% of running speeds were excluded from the correlation.

Theta modulation was calculated by assigning each spike of a given cell to the phase of the LFP theta at which it occurred. Theta phases were plotted in a polar plot and modulation strength was taken as the MRL.

## 2.6 | Spatial correlation, firing rate overlap, score similarity, and comparisons across time

For all calculations, only pairs of rate maps from identical configurations of the open field were compared. We calculated the spatial similarity between two rate maps using Pearson's correlation between the firing rates of bins at corresponding locations. Any bins that were unvisited in either map were excluded from the calculation. Firing rate overlap was calculated for each rate map as: $1 - \frac{|R1 - R2|}{R1 + R2}$ where *R1* is the mean firing rate from map 1 and *R2* is the mean firing rate from map 2. For grid cells, firing rate overlap was calculated independently for each grid field and the values were averaged across all fields of a given grid cell.

To compare the similarity of grid scores, speed scores, and HD MRL values we calculated the absolute value of the change between two sessions. This difference was then subtracted from 1 to yield a "similarity value" of the score. Thus, for grid scores, a similarity of 1 means no difference in raw grid score between two sessions while a similarity of 0.7 means that the raw grid score changed by 0.3 between the two sessions (e.g., 1.3 in session 1 and 1.6 in session 2). As such, systematic drift in a score over time would be reflected by a progressive decrease in similarity (i.e., negative slope).

Recording the same cell multiple times yields many pairwise comparisons that all share the same temporal delay. For example, across the four recording sessions in a block there are three different pairwise comparisons of adjacent sessions (session 1 vs. 2, 2 vs. 3, and 3 vs. 4). Because some cells were recorded for longer than others, not all cells had an identical number of pairwise comparisons for a given temporal delay. Thus, to make sure that all cells contributed evenly to all analyses when making any temporal comparison, we collected all corresponding pairwise rate maps for a given cell and randomly drew a single pair, meaning that each cell was included in an analysis exactly one time, regardless of the total amount that a cell had been recorded. As this method meant that each individual calculation was influenced

by the nature of the random draw, we repeated each calculation 25 times for each cell and time interval, performing a new random draw each time. The 25 repetitions were then averaged to a single value for that cell and time interval. Note that in most cases 25 iterations exceeded all possible pairwise comparisons but that taking the average of randomly repeating comparisons would not bias the final value for the cell.

### 2.7 | Chance level comparisons

For spatial correlation and rate overlap comparisons, we calculated chance level values by shuffling cell identities. Instead of comparing the same cell across sessions at two different time points, each cell was compared to any other recorded cell selected at random. Just as in the case of our standard calculations, this random matching across cell identities was performed 25 times and averaged to yield a single chance level value for each cell. This procedure provided chance level similarity for each of the time intervals. In all cases, calculations of chance values and shuffling of cell identities were performed independently for the population of grid and non-grid cells (border and irregular spatial cells combined). This was done due to the periodic nature of the spatial firing of grid cells and because the calculation of firing rate overlap was different between the two groups (per field for grid cells and across the entire map for non-grid cells).

### 2.8 | Statistics

For comparing isolation distances, we used a KS-Test to compare the full data set to the subset of cells that were tracked over at least two recording blocks and to compare the isolation distance between the first and the last recording of those cells that were tracked. All comparisons between groups (WSC, SI, change in spatial correlation, change in rate overlap, similarity of grid score, speed score, or HD modulation) were made using either a Mann–Whitney rank-sum test when comparing two groups, or a Kruskal-Wallis test with Tukey's HSD post hoc when comparing three or more groups. SI and WSC values were corrected by subtracting each cell's chance levels which were obtained by calculating the corresponding values from shuffled data (ΔSI and ΔWSC). Comparisons between median shifted WSC and SI distributions were made using a KS-Test. Comparisons of slope values (change over time) to zero were made using a Wilcoxon signed-rank test. When sample sizes were small ($n < 15$) an exact test statistic was calculated for the rank-sum and signed-rank tests. For data recorded from the small environment, changes between shapes made it such that for some cells and temporal lags it was not possible to make a comparison between identical environments. Therefore, comparisons were made using a Skillings-Mack test for repeated measure with missing data (Skillings and Mack, 1981) with a rank-sum test for post hoc analysis. Determination of the subset of non-grid cells that exhibited significant changes to their firing patterns over 6 hrs was made by comparing calculated changes over time (Figure 4d) to chance calculations based on shuffled cell identities. Cells that systematically varied over time were identified as those exhibiting change values below the 2.5th percentile of the shuffled distribution (equivalent to $\alpha = 0.05$ for two-tailed statistics). For any evaluation of correlation between two variables a Pearson's correlation was performed, although in all cases a Spearman's correlation yielded statistically equivalent results. Comparisons of proportion of cells between Layers 2 and 3 were done using Pearson's chi-square test for categorical data. All statistical comparisons were significant at $p < .05$ for two tailed distributions.

## 3 | RESULTS

### 3.1 | Principal cells from mEC superficial layers were recorded across multiple sessions within a day

To evaluate the stability of mEC spatial firing patterns over time, we trained rats to randomly forage in an open field arena for eight 10-min sessions within a day. Rats were trained to either explore two small enclosures (an 80 cm by 80 cm square and a 100 cm-diameter circle) or to explore one large enclosure (a 120 cm by 120 cm square). In the morning of each day, rats performed a block of four 10-min foraging sessions that were each separated by 5-min rest sessions. The morning block was followed by a 6-hr break, after which rats performed another block of four 10-min foraging sessions in the afternoon. Between the morning and afternoon blocks rats were returned to their home cage. This design allowed us to evaluate the consistency of mEC firing ($n = 313$ principal cells; Figure 1a,b) within a single 10-min session, across a series of sessions spanning roughly 1 hr, and between sessions separated by several hours.

To compare the spatial firing patterns between sessions in the same environment, we used previously published techniques to track the same set of cells across multiple recording sessions (Mankin et al., 2015; Mankin et al., 2012). Briefly, a spike cluster was identified as an individual cell when the cluster remained in the same location in multidimensional cluster space over a series of recording sessions as determined by applying the same cluster bounds across sessions, and when the cluster was clearly separable from all other clusters in each recording session within the series (Figure 1c,d). Identified cells were tracked for as long as possible, ranging from a single block of four sessions to 10 recording blocks spanning five days. Cells were tracked until there was no longer a spike cluster remaining in the tracked cluster space for multiple behavioral or sleep sessions. While such a lack of spiking could reflect periods of cellular inactivity during behavior, as has been described in CA1 (Thompson and Best, 1989), we never observed instances in which clusters were only detected in sleep sessions. We also did not observe the disappearing and reappearing of clusters during repeated behavioral sessions, contrary to previously described observations for CA1 recordings under similar conditions (Mankin et al., 2012). This observation is consistent with previous reports that the same mEC cells that are active during sleep periods are also active during exploration of an environment (Fyhn et al., 2004).

To quantify the quality of our single-unit clusters we calculated the isolation distance in each session (Figure 1e). While we did not exclude data based on isolation distance, 99.5% of our clusters would be identified as high quality (isolation distance >10) based on previous criteria for mEC recordings (Newman and Hasselmo, 2014; Perez-Escobar et al., 2016). We compared the isolation distance between

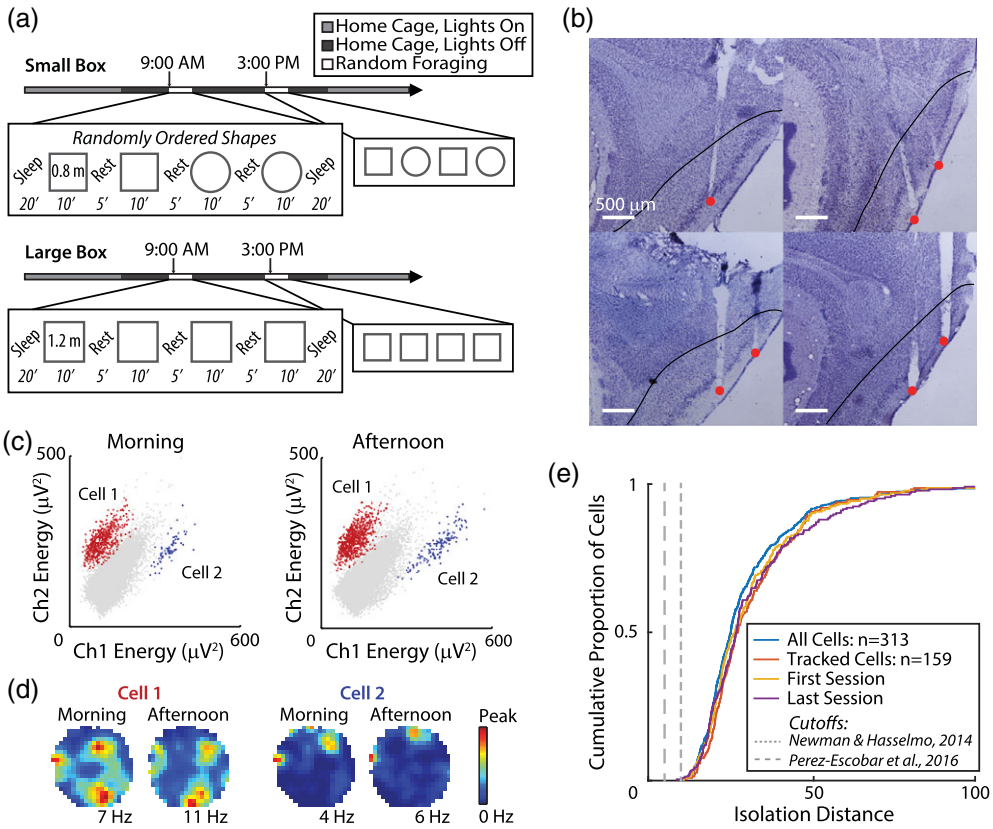


**FIGURE 1** Medial entorhinal cells were recorded across multiple sessions in either small or large environments. (a) Schematic of the two experimental paradigms. Rats repeatedly randomly foraged in the same open field environment. A block of four sessions in the morning was followed by a block of four sessions 6-hr later. Each foraging session within a block lasted 10-min with 5-min rest periods in between. Individual mEC cells were tracked across sessions and blocks. Three rats explored a small environment with flexible walls that were configured as either a square (80 cm by 80 cm) or a circle (100 cm diameter). Note that for this study all comparisons were between sessions in like-shaped environment configurations. The remaining five rats explored a single large square environment (120 cm by 120 cm). (b) Example histological sections of mEC tetrode tracks from four rats. The superficial layers are delineated by the black line and the end of each tetrode track is marked with a red dot. Scale bars = 500 µm. (c) Examples of two well isolated clusters that were tracked across sessions in the morning and afternoon. Each cluster remained in the same location in multidimensional cluster space allowing for the determination that each represented a single cell tracked across the day. (d) Rate maps of the tracked cells from c. Firing rates are color-coded according to the scale bar on the right and the peak rate is noted below each map. Both cells maintain similar spatial firing patterns across the day, but rate maps were never used for cell tracking. (e) Cluster isolation distance was calculated for all recorded mEC cells and for only those cells that were tracked over multiple recording blocks. Of those cells that were tracked, we also calculated the isolation distance the first and the last time that the cell was recorded. The distribution of isolation distances was comparable across all four conditions. While we did not use any quantitative threshold for our clusters, over 99.5% of our clusters have an isolation distance in excess of previously published cutoffs (isolation distance of 5 or 10; dashed gray lines) [Color figure can be viewed at wileyonlinelibrary.com]

the full population of recorded cells and the subset of cells that were tracked across multiple recording blocks and did not find a difference (ks = 0.098, $p > .05$). We also found no difference in isolation distance between clusters from the first and the last recording session of tracked cells (ks = 0.069, $p > .05$) (Figure 1e).

## 3.2 | The spatial content of mEC cells depended on the size of the environment

In both our small and our large environment, we identified grid cells, border cells, as well as a population of irregular cells (firing not in a grid pattern or along a wall) with a wide range of spatial firing patterns (Figure 2a). Within our small environment, we only detected four border cells so this population was not analyzed further. Whereas some irregular cells had highly precise spatial firing patterns, the firing of other irregular cells was considerably more diffuse. To quantify each cell's spatial firing pattern, we calculated the spatial information (SI: a metric of the level of spatial content conveyed by each spike) and the within session correlation (WSC: a metric of the stability of the spatial firing pattern within a single 10-min session) (Figure 2b-e). These two metrics were adjusted by subtracting each cell's chance activity (ΔSI or ΔWSC).

Using these metrics for comparisons of spatial firing patterns in single 10-min recording sessions yielded three main results, all of which matched with our subjective observations of the spatial firing properties of mEC cells. First, spatial firing of grid cells and border cells was comparable and was more precise and consistent than that of irregular cells (small box, grid vs. irregular, ΔSI,: $z = 3.89$, $p < .001$; ΔWSC,: $z = 4.39$, $p < .001$; large box, grid vs. border vs. irregular, ΔSI: Chi-Sq[2] = 38.50, $p < .001$; post hoc, grid vs. irregular and border

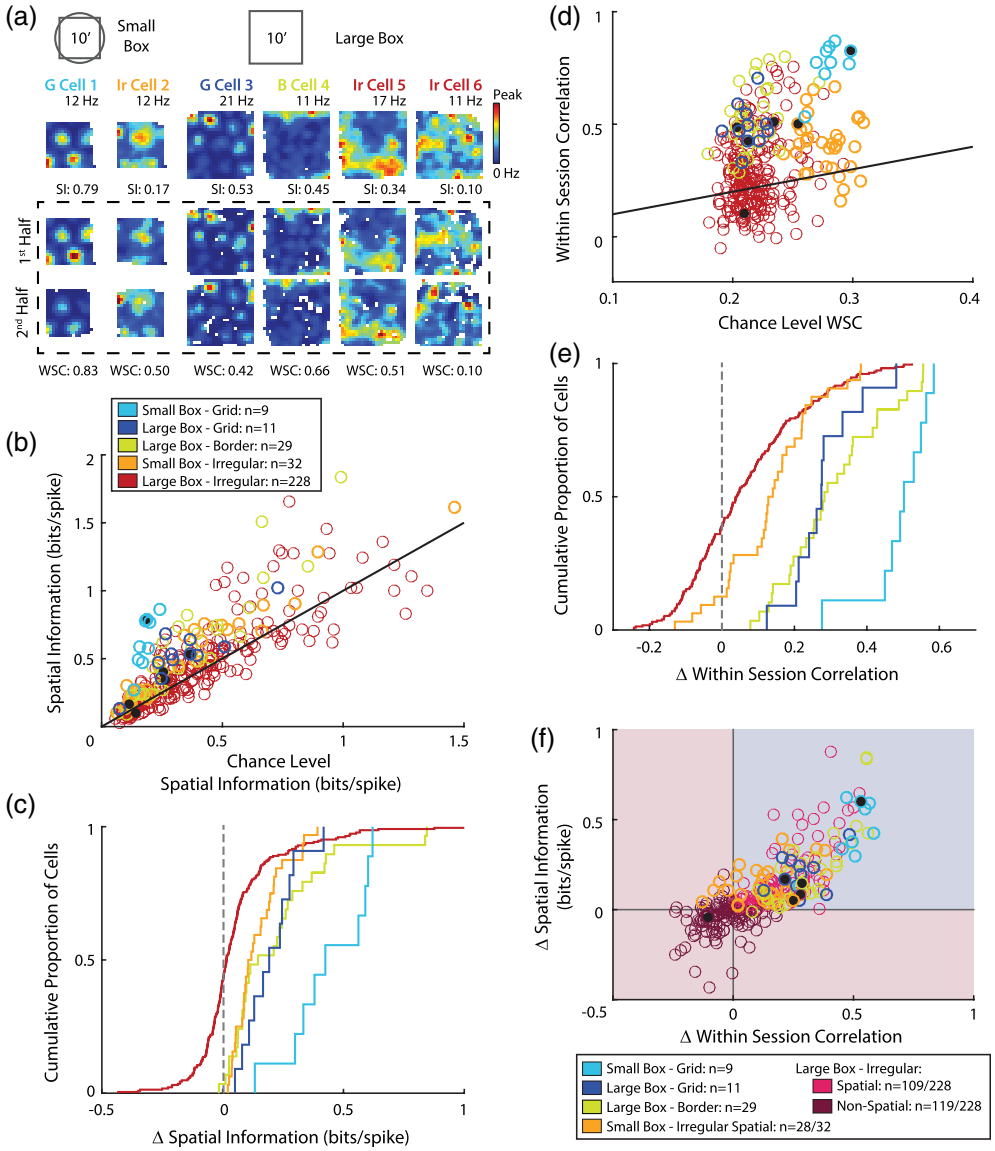


**FIGURE 2** The spatial firing patterns of mEC cells were reliable within a single 10-min session. (a) Rate maps of example grid, border, and irregular cells recorded from the two environment sizes. Firing rates are color-coded according to the scale bar on the right. For each rate map, the peak rate is noted above and SI is noted below. In the box marked by the stippled line, rate maps from each cell are shown separately for the first and second half of the 10-min behavioral session, and the WSC is noted below each pair. The example cells are identified in the scatter plots in (b), (d), and (f ) as solid black circles. G, grid cell. Ir, irregular cell. B, border cell. (b) Average SI of mEC cells in a single 10-min session as a function of the chance level SI based on shuffling procedures. Data are segregated based on box size and by grid, border, and irregular cells. (c) CDFs of the difference between the actual SI and chance-level SI (ΔSI). (d) Average WSC of mEC cells in a single 10-min session as a function of chance level WSC. (e) CDFs of the difference between actual WSC and chance-level WSC (ΔWSC). (f ) ΔSI is plotted as a function of ΔWSC for each recorded mEC cell. Despite ΔSI and ΔWSC quantifying different aspects of the spatial firing patterns of a cell, the two were highly correlated ($r$ = .78, $p = 1.89 \times 10^{-65}$). Cells were identified as spatial if both SI and WSC were above chance (blue quadrant) and as nonspatial if WSC and/or SI was below chance (red quadrants). All grid and border cells in the small and large environment and most irregular cells in the small environment were classified as spatial. However, about half of the irregular cells in the large environment (119 of 228) were nonspatial [Color figure can be viewed at wileyonlinelibrary.com]

vs. irregular, both $p$ < .001; grid vs. border, n.s; ΔWSC: Chi-Sq [2] = 54.19, $p$ < .001; post hoc grid vs. irregular and border vs. irregular, both $p$ < .001; grid vs. border, n.s.). Second, spatial firing patterns of both grid and irregular cells that were recorded in the small environment were more precise than spatial firing patterns of cells recorded in the large environment (small vs. large box, grid, ΔSI: $z$ = 2.96, $p$ < .01; irregular: $z$ = 5.04, $p$ < .001; small vs. large box, grid, ΔWSC: $z$ = 3.27, $p$ < .01; irregular: $z$ = 2.75, $p$ < .01). Interestingly, the size of the environment did not alter the shape of the SI or WSC distributions, but instead lead to a simple scalar decrease in the level of spatial firing across all mEC cells. After shifting both distributions to a median of 0 there was no difference in the distributions of data recorded in the small and large environments (small vs. large box, grid, SI: ks = 0.35, $p$ > .05; irregular: ks = 0.14, $p$ > .05; small vs. large box, grid, WSC: ks = 0.18, $p$ > .05; irregular: ks = 0.15, $p$ > .05). Due to the fact that data from the two environment sizes were recorded from different rats it is possible that differences in anatomical recording location could explain the difference in spatial firing properties.

However, tetrodes were targeted to the same location in all rats, and recordings came from broad, highly overlapping regions across all animals. Furthermore, within each animal there was considerable intermixing of cells with high and low SI and/or WSC, with many instances of simultaneous recordings of high and low values on the same tetrode, making anatomical location an unlikely explanation for the differences between box sizes. Third, whereas about 90% of mEC cells recorded in our small environment exhibited spatial firing patterns in excess of what would be expected by chance (i.e., ΔSI and ΔWSC >0), the proportion of significantly spatial cells was reduced to ~55% for cells recorded in the large environment. For further examination of the stability of spatial firing of mEC cells, we segregated irregular cells into two groups: those with SI and WSC above chance levels (spatial) and those with SI and/or WSC below chance level (nonspatial) (Figure 2f). Taken together, mEC cells were generally less spatial in a larger environment, such that a larger proportion of cells were characterized by spatial firing below chance levels.

### 3.3 | Medial entorhinal cortex cells were stable across tens of minutes

After establishing that the majority of mEC cells exhibited spatial firing patterns that were reliable over the course of a single 10-min recording session, we next asked whether mEC firing patterns were consistent when rats randomly foraged in the same environment repeatedly. As each of our recording blocks consisted of four open field foraging sessions, it was possible to compare the similarity of spatial representations between sessions as a function of the temporal distance between them, which corresponded to either 15, 30 or 45 min (Figure 3a). Past work has shown that in the hippocampus, CA1 and CA3 place cell representations remain highly stable over the course of an hour, while CA2 cells already begin to exhibit substantial changes after only 15 min (Mankin et al., 2015). Thus, we sought to determine whether the trajectory of stability of mEC representations over time resembled either the stable time invariant CA3 representations or the time varying CA2 representations.

While we observed that the similarity of spatial firing patterns across sessions was highest in grid cells and lowest in irregular nonspatial cells, across all groups of cells both the spatial firing patterns and the overall firing rate of mEC cells were just as similar between sessions separated by 45 min as when sessions were separated by only 15 min (Figure 3b,c). Although the spatial correlation between sessions varied across individual cells and across cell classes (grid, border, irregular spatial, irregular nonspatial), individual cells exhibited considerable consistency in their spatial correlation values across all three lags. Furthermore, even cells that had been classified as nonspatial based on activity within a single session had spatial correlations across sessions in excess of chance levels, suggesting that our classification criteria were overly conservative and that in fact virtually all mEC cells exhibited measurable spatial firing patterns across repetitions of the same environment.

For mEC cells recorded in the single large environment, we quantified the degree of change in spatial correlation and rate overlap over time (i.e., the trajectory of stability) by fitting the data of each cell across the three time lags with a linear regression and calculating the slope of the fit line (Figure 3d). We found that the rate of change in spatial correlation was not different from zero for all four groups of mEC cells (grid: signed-rank = 28; border: $z = 1.94$; irregular spatial: $z = -1.93$; irregular nonspatial: $z = -1.50$; all $p$ values >.05) as was the case for the rate of change in firing rate overlap for grid cells (signed-rank = 16, $p > .05$). Border cells as well as both groups of irregular cells had significant decreases in firing rate overlap over time (border: $z = -2.19$, $p < .05$; irregular spatial: $z = -4.17$, $p < .001$; irregular nonspatial: $z = -3.91$, $p < .001$), but in each case the average decrease was less than 5% over the course of three behavioral sessions. Additionally, we found no differences in slope values between the four mEC cell types recorded in the large box for spatial correlation (grid vs. border vs. irregular spatial vs. irregular nonspatial: Chi-Sq [3] = 6.96, $p > .05$) or rate overlap (Chi-Sq[3] = 0.97, $p > .05$) indicating that all cell types had comparable levels of firing stability over tens of minutes.

For the subset of cells that were recorded in the small environment, alternating between two shapes meant that it was not always possible to compare between identical environments at all three temporal lags. For example, for a recording block with the order [Square, Circle, Circle, Square] it would be possible to evaluate firing with Lag 1 (between circles) and Lag 3 (between squares), but there would be no comparison in which identical environments were separated by Lag 2. Thus, for these data only group averages at each lag are presented and statistical considerations were taken to account for missing data points (see methods). For both grid and irregular spatial cells recorded from the small environment, there was no systematic decrease in spatial correlation or firing rate overlap when comparing the three temporal lags (spatial correlation, grid: $t(2) = 0.88$, $p > .05$; irregular spatial: $t(2) = 8.55$, $p < .05$, Lag 1 vs. Lag 3 $p > .05$; rate overlap, grid: $t(2) = 2.49$, $p > .05$; irregular spatial: $t(2) = 0.64$, $p > .05$). As there were only five irregular cells recorded in the small environment with spatial firing below chance (nonspatial), this group was not analyzed. While data for these analyses were combined between both the square and circle shaped enclosures, we observed the same results when examining data from each shape separately. Furthermore, baseline levels (i.e., Lag 1 comparisons) of spatial correlation and rate overlap were not different between the square enclosure and the circular enclosure (spatial correlation at Lag 1, square vs. circle, grid: rank-sum = 58; irregular: $z = 1.80$; rate overlap at Lag 1, square vs. circle, grid: rank-sum = 58; irregular: $z = 0.07$; all $p$ values >.05).

Lastly, we sought to compare the stability of the spatial firing of mEC cells between sessions to the stability within a single 10-min session (Figure 3e). WSC and spatial correlation across pairs of rate maps separated by Lag 1 were highly correlated ($r = .89$, $p = 4.83 \times 10^{-106}$) indicating that those cells that tended to have more consistent spatial firing within a single session also had more consistent firing across repeated exposures to a given environment. A similar pattern was observed when comparing WSC to spatial correlation across Lag 3 ($r = .80$, $p = 6.75 \times 10^{-69}$), further supporting our finding that the spatial firing of mEC cells did not change systematically over tens of minutes.

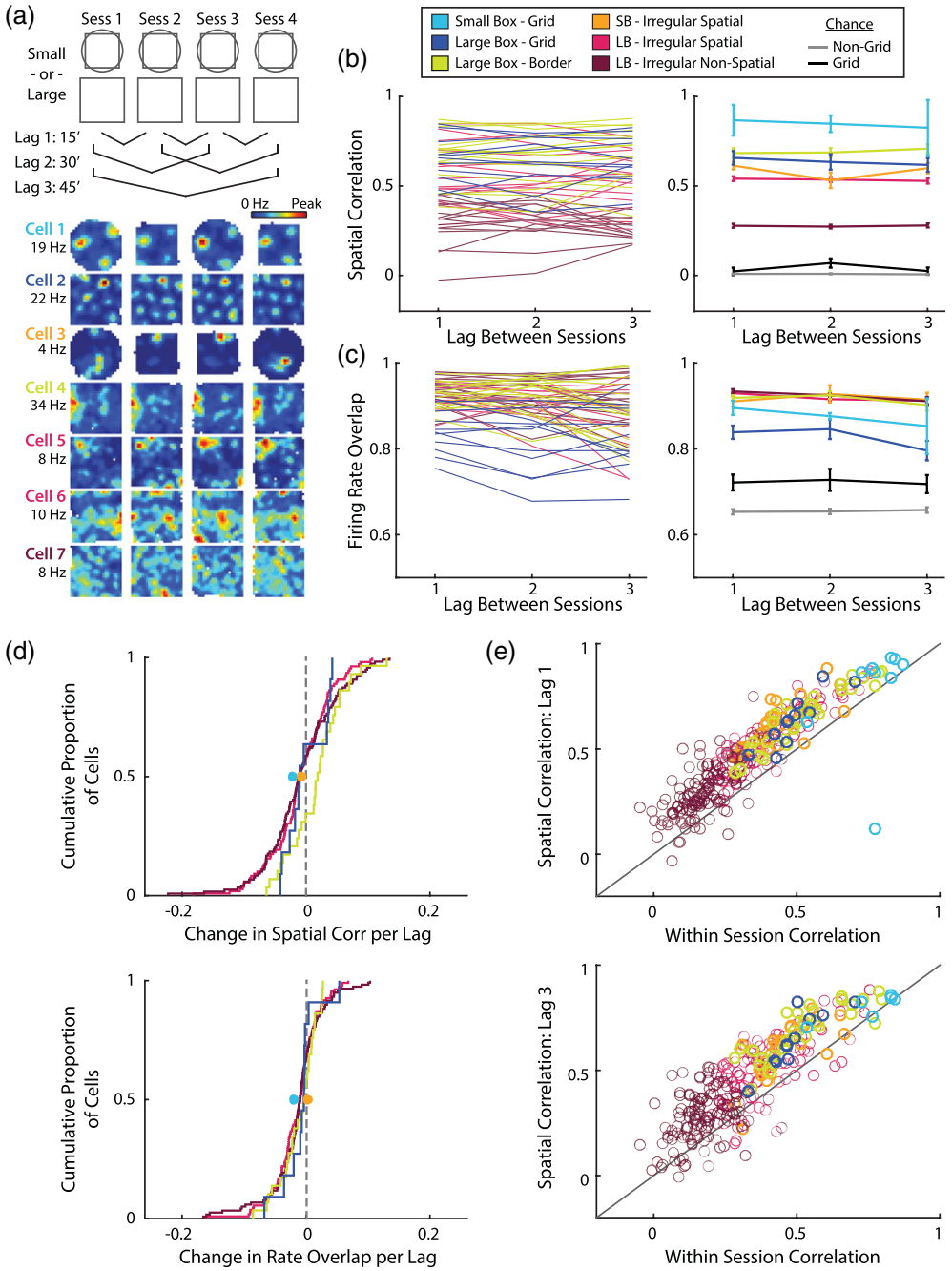


**FIGURE 3** Medial entorhinal cortex representations were stable across tens of minutes. (a) Schematic of potential comparisons for evaluating changes within a block of four sessions, and rate maps of seven example cells across the four sessions. Font color for each rate map label corresponds to the legend in (b). Firing rate maps were compared between adjacent sessions (Lag 1), between sessions that are two apart (Lag 2), or between sessions that are three apart (Lag 3). (b) Spatial correlation of mEC cells across lags of 1, 2, or 3 sessions. Data are segregated based on environment size (small box: SB; large box: LB) and grid, border and irregular cells. Irregular cells recorded from the large environment are further segregated into spatial and nonspatial groups (see Figure 2f). Left, spatial correlation values of individual cells in the large environment. A random subset of up to 15 cells per group was selected for illustration purposes. As the order of the shape presentation in the small environment was varied, not all lag comparisons were available for each cell. Thus, individual cell data do not include cells from the small environment. Right, group median ± SEM for mEC cell types in the small and large environments. Chance level correlations were calculated for grid and non-grid cell populations by repeating the same calculations after shuffling cell identities. (c) Firing rate overlaps of mEC cells across lags of 1, 2, or 3 sessions presented as in B with individual cells on the left and group averages on the right. Rate overlap values for grid cells were calculated for each grid field and averaged across all fields of a grid cell. (d) Changes in spatial correlation and firing rate overlap over time were calculated for each cell by taking the slope of the best fit line of data in (b) and (c). CDFs of the change over time are shown for data recorded from the large environment. For data from the small environment, population average values were used to calculate changes over time and are presented as a single point per group. (e) Spatial correlation for each cell across sessions separated by Lag 1 (top) or Lag 3 (bottom) are shown as a function of the average WSC of the cell [Color figure can be viewed at wileyonlinelibrary.com]

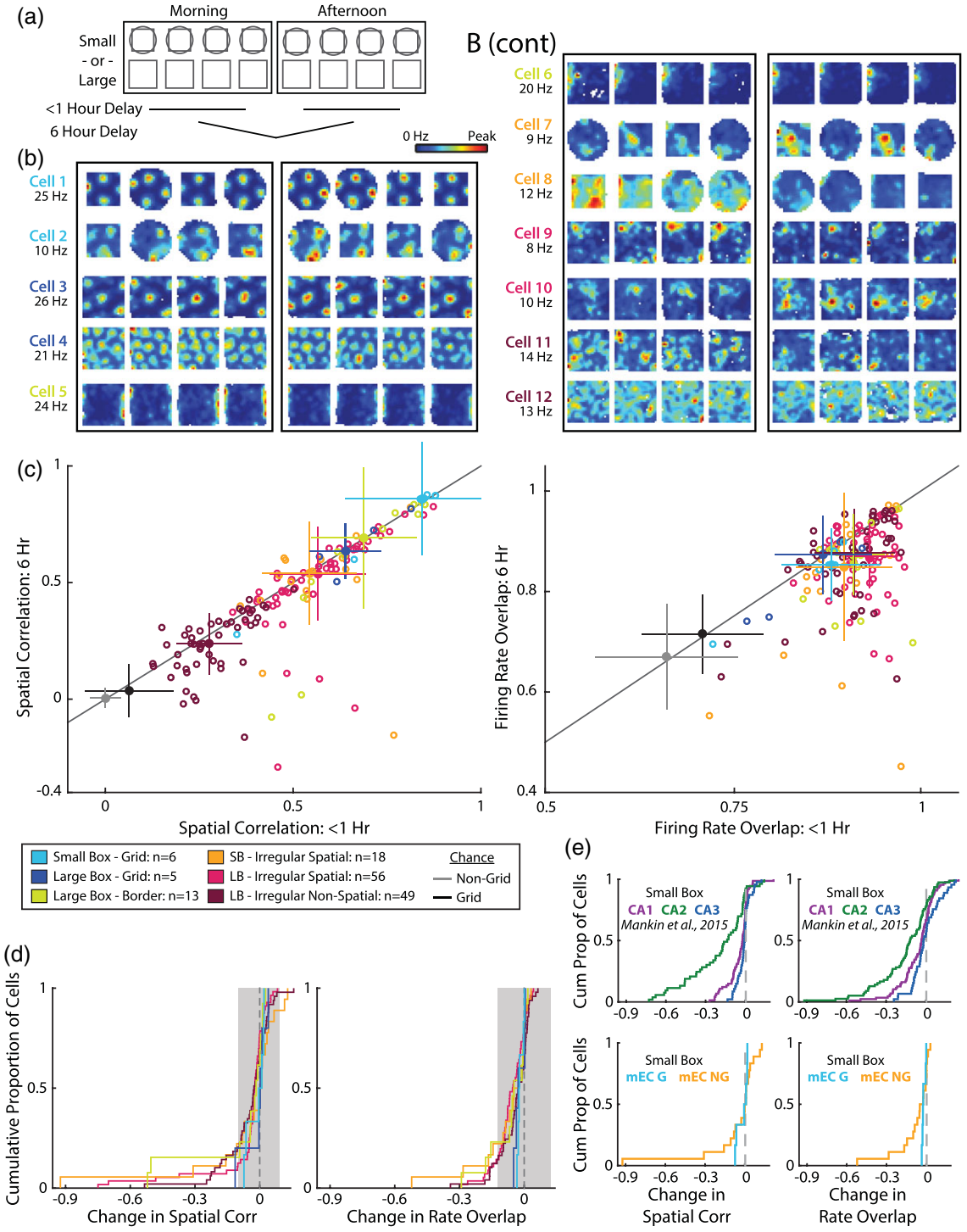


### 3.4 | Firing patterns of grid cells and the majority of non-grid cells were stable over 6 hrs

After observing that mEC representations did not change across intervals of less than 1 hr, we determined whether representations were stable over the course of several hours. As we were able to track the identity of a subset of our mEC cell population from the morning to the afternoon (159 of 313 cells), it was possible to compare their firing properties between sessions separated by less than 1 hr (either within the morning or afternoon block) and between sessions that were separated by 6 hrs (between the morning and afternoon block) (Figure 4a). In general, mEC cells appeared to be largely consistent in their firing patterns from the morning to the afternoon, exhibiting approximately the same spatial firing patterns at comparable firing rates (Figure 4b). To quantify the stability of mEC firing, we compared spatial correlations and firing rate overlap values between rate maps separated by less than 1 hr and those separated by 6 hrs (Figure 4c). We also calculated the change over time (Figure 4d), although this was simply the difference between the two time points, as opposed to the slope of a fit line as calculated for Figure 3d. Our first observations were that the firing characteristics of mEC grid cells over time were not influenced by the size of the recording environment (small box vs. large box for change in spatial correlation: rank-sum = 37, $p > .05$; change in rate overlap:

rank-sum = 36, $p > .05$). For our groups of non-grid cells, there were neither differences depending on the size of the environment nor depending on whether cells were classified as border, irregular spatial, or irregular nonspatial in the large box (irregular spatial small box vs. border large box vs. irregular spatial large box vs. irregular nonspatial large box, change in spatial correlation: Chi-Sq[3] = 1.35, $p > .05$; change in rate overlap: Chi-Sq[3] = 2.01, $p > .05$). Thus, for subsequent statistical comparisons we grouped all grid cells together and all non-grid cells together regardless of environment size, cell classification, or degree of spatial firing. Additionally, while data from the small enclosure were combined between square and circular shaped environments, we found that, when examined separately, data recorded from the square shaped enclosure and data from the circular enclosure were comparable and that the cells' baseline spatial similarity was not different between the two shapes (spatial correlation <1 hr, square vs. circle, grid: rank-sum = 51; irregular: $z = -0.76$; rate overlap <1 hr, square vs. circle, grid: rank-sum = 40; irregular: $z = 0.60$; All $p > .05$).

In evaluating firing over 6 hrs, we found that the spatial firing pattern and overall firing rate of mEC grid cells was stable over time (change in spatial correlation vs. zero: signed-rank = 30, $p > .05$; change in rate overlap vs. zero: signed-rank = 19, $p > .05$). Such high stability is in stark contrast to the rapid decorrelation over time that we previously described for the hippocampal CA2 region (Figure 4e; Data reanalyzed from Mankin et al., 2015 and presented for comparison). As a complement to our analysis of the spatial firing patterns of grid cells, we also examined whether grid scores (a numerical evaluation of hexagonal periodicity) of our grid cell population changed as a function of time (Figure 5). We compared the similarity of grid score values across tens of minutes (Figure 5a) or across 6 hrs (Figure 5d) and calculated the degree of change over time to determine if sessions separated by longer periods of time would have grid scores that were more dissimilar than sessions separated by shorter periods (Figure 5b,e). Just as for spatial correlation and firing rate overlap we found no systematic changes in grid scores over either short (small box, difference in similarity across lags: $t(2) = 0.38$, $p > .05$; large box, change in similarity vs. zero: signed-rank = 30, $p > .05$) or long time periods (small box, change in similarity vs. zero: signed-rank = 11, $p > .05$; large box: signed-rank = 6, $p > .05$). Furthermore, for both timescales we observed no relationship between a cell's average grid score and its degree of change over time (minutes, large box: $r = .23$; hours, small box: $r = .08$; hours, large box: $r = -.21$; all $p$ values >.05) (Figure 5c,f). Thus, the quantitative periodicity, firing rates, and spatial firing patterns of grid cells all remained highly stable over elapsed time.

Whereas the firing patterns of all grid cells remained stable over time, we observed a clear negative tail in the distribution of non-grid cells for both spatial pattern and firing rate change (Figure 4e). As such, the average change in spatial correlation or rate overlap of the non-grid cell population was significantly below zero (change in spatial correlation vs. zero: $z = -5.17$, $p < .001$; change in rate overlap vs. zero: $z = -6.66$, $p < .001$). To determine which non-grid cells exhibited substantive changes over time, we compared the change in spatial correlation or rate overlap to chance distributions generated by performing the exact same calculations but shuffling cell identities such that pairwise comparisons were across different cells (see methods). We could then compare the behavior of non-grid cells to chance, identifying those cells with a degree of change below the 2.5th percentile ($\alpha = 0.05$ for two-tailed statistics) as exhibiting a systematic decrease in their spatial correlation or rate overlap. Using this method, we observed that 16% of non-grid cells exhibited significant changes as a function of time in their spatial firing pattern and that 16% exhibited changes over time in their overall firing rate, leaving a large portion of the non-grid cell population that were not characterized by systematic changes in firing patterns over time. Furthermore, the proportions of cells that changed were comparable across environment size, cell classification, and degree of spatial firing (irregular spatial, small box: 17% and 22% for space and rate change; border, large box: 15% and 23%; irregular spatial, large box: 9% and 14%; irregular nonspatial, large box: 24% and 14%).

**FIGURE 4** Medial entorhinal cortex grid cells and most non-grid cells were stable over time but a subset of non-grid cells changed. (a) Schematic of comparisons between rate maps separated by less than 1 hr or with a 6-hr delay. (b) Rate maps of 12 example cells that were tracked from the morning to the afternoon sessions. Font color for each rate map label corresponds to the legend in (c). For cells that were recorded in both a square and a circular enclosure, only sessions in identical shapes were compared. In general, the spatial firing patterns of mEC cells remained similar over the course of the day. However, a few cells exhibited major changes in their firing patterns. (c) Spatial correlation (left) and firing rate overlap (right) for mEC cells. Scatter plots for each of these measurements are between rate maps separated in time by less than 1 hr and rate maps separated by 6 hrs. Data are color-coded by environment size (small box: SB; large box: LB) and by grid, border, and irregular cells. Irregular cells that were recorded in the large environment are further divided into spatial and nonspatial cells. The median values for each group are shown as a filled circle $\pm$ standard deviation. Chance levels are plotted for grid and non-grid populations as determined by shuffling cell identities. (d) The change in spatial correlation and firing rate overlap over time was calculated for each cell by taking the difference between comparisons across less than an hour and comparisons across 6 hrs. Difference values were also computed for the chance calculations to yield a null distribution of change over time. The chance distribution of the non-grid cell population is plotted as the shaded region spanning between the 2.5th and 97.5th percentiles of the distribution. Cells with a value outside of this region would be identified as those with significant change over time. (e) Top, previously published recordings of hippocampal cells across 6 hrs in a small environment (Mankin et al., 2015) were reanalyzed with the same methods as used here for mEC data. Bottom, mEC data from the small environment are redrawn from panel (d) (grid: G; non-grid: NG). Note that the spatial correlations of hippocampal cells at short time intervals are generally considerably higher than that of mEC non-grid cells although non-grid cells nonetheless have sufficiently high correlation values to preclude floor effects (see spatial correlation values in Figures 3b and 4c). Here, we are plotting the relative change over time with respect to each brain region's respective baseline. Thus, values reflect relative change, not absolute similarity. While these plots allow for an approximate comparison between mEC and hippocampal data, direct statistical comparisons were not made due to low mEC cell numbers, lack of any simultaneous recordings between the two regions, and the fundamentally different spatial firing patterns between hippocampal place cells and mEC grid and non-grid cells [Color figure can be viewed at wileyonlinelibrary.com]

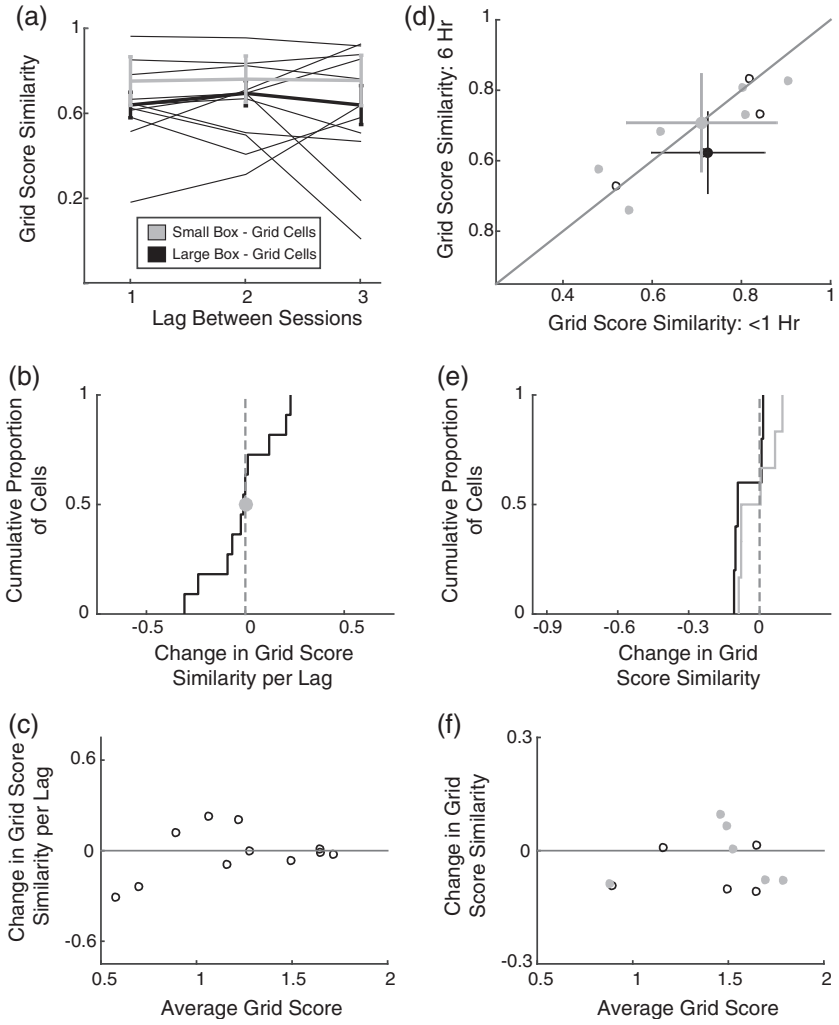


**FIGURE 5** Grid scores did not vary systematically over time. (a) Similarity of grid scores of mEC grid cells across lags of 1, 2, or 3 sessions and (b) the change over time are plotted as in Figure 3. Grid score similarity was calculated as 1 minus the absolute value of the difference between raw grid scores in two sessions. Thus, a similarity value of 1 indicates no change in raw grid score and a value of 0.7 indicates that grid score changed by 0.3 between sessions. Data for the two environment sizes are shown separately. (c) Change in grid score similarity for data recorded from the large environment is plotted as a function of the cell's average grid score across all recorded sessions. (d, e) similarity of grid scores of mEC grid cells across sessions separated by less than 1 hr or 6 hrs are plotted as in Figure 4. (f ) Change in grid score similarity across 6 hrs is plotted as a function of the cell's average grid score across all recorded sessions

## 3.5 | Speed and head direction tuning of mEC cell populations remained stable over time

While our analysis thus far has categorized mEC cells according to their spatial firing patterns (grid, border, and irregular), mEC cells can also be strongly modulated by an animal's heading direction (HD) or running speed (Kropff et al., 2015; Sargolini et al., 2006). To determine whether representations of HD or running speed varied systematically over time we adapted our analysis to compare the similarity of HD mean resultant length (MRL) values and speed scores across sessions separated by tens of minutes (Figure 6) or across sessions separated by 6 hrs (Figure 7). As HD or speed modulation occur in conjunction with spatial modulation in grid, border, or irregular cells, we performed these analyses on our entire population of mEC cells, irrespective of any functional classification. In examining HD and speed score across our short time period (Figure 6a,b), we found no difference in score similarity across lags for mEC cells recorded in the small enclosure (HD: $t(2) = 4.68$, $p > .05$; speed score: $t(2) = 0.64$, $p > .05$). For recordings in the large enclosure the decrease in score similarity over tens of minutes reached significance (HD: $z = -1.99$, $p < .05$; speed score: $z = -2.36$, $p < .05$), although the magnitude of the change was small. Furthermore, there was no significant relationship between a cell's average HD or speed score and the change in the value over time (HD: $r = -.08$, $p > .05$; speed score: $r = -.04$, $p > .05$) (Figure 6c) indicating that those mEC cells that might be identified as HD or speed cells had no increased propensity to vary their respective firing characteristics systematically over time. In tracking the same cells across a 6-hr period, we found no significant change over time in HD or speed modulation (Figure 7a,b). For both HD and speed scores, the decrease in similarity over 6 hrs was no different from zero (HD, small box: $z = -0.92$; large box: $z = -0.13$; speed score, small box: $z = -0.44$; large box: $z = -1.37$; All $p > .05$). Additionally, for both metrics there was no relationship between a cell's average value and the change over time (HD, small box: $r = .21$; large box: $r = -.03$; speed score, small box: $r = -.07$; large box: $r = .06$; All $p > .05$) (Figure 7c).

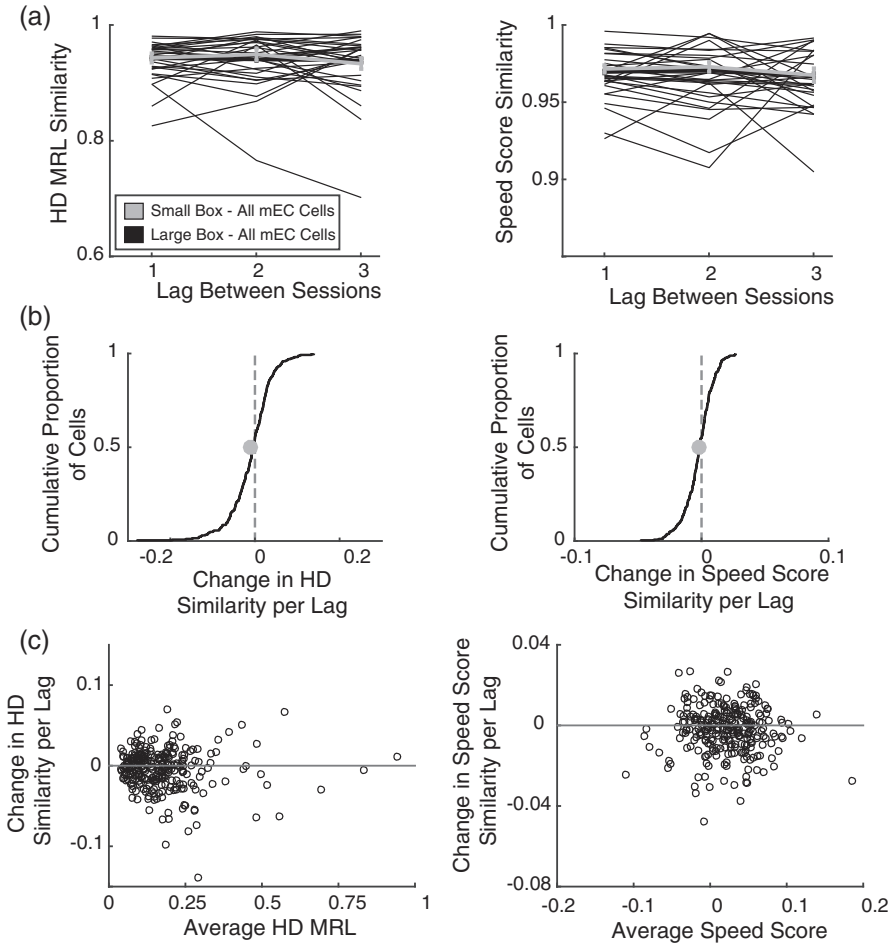


**FIGURE 6** Head direction and speed modulation did not vary systematically over tens of minutes. (a, b) Similarity of HD modulation (left) and speed scores (right) of all mEC cells across lags of 1, 2, or 3 sessions (a) and the change over time (b) are plotted as in Figure 3. Similarity values for HD and speed score are calculated as for grid scores. Data for the two environment sizes are shown separately. (c) Change in HD modulation (left) and speed score similarity (right) for data recorded from the large environment are plotted as a function of the cell's average across all recorded sessions

Therefore, speed and HD tuning of mEC cell populations did not systematically vary over time.

## 3.6 | Non-grid cells that changed over time were preferentially recorded from Layer 3 over Layer 2

Having identified that any systematic changes over time within the mEC network were restricted to the spatial firing or overall firing rate in a subset of the non-grid cell population, we sought to gain further insight into this group of cells. We first verified that our observed changes over time were not a consequence of poor single unit cluster cutting procedures as there was no relationship between changes over time and changes in a cell's isolation distance (change in spatial correlation: $r = .06$, $p > .05$; change in rate overlap: $r = .01$, $p > .05$) (Figure 8a). Next, we sought to determine whether there were any firing properties that may identify non-grid cells that change over time as a distinct subset of the mEC population. We did not observe any relationship between changes over extended time and a cell's average firing rate, waveform shape, strength of theta modulation, spatial information, or within session correlation (change in spatial correlation: $r$ ranged from −.14 to .08, all $p > .05$; change in rate overlap: $r$ ranged from −.11 to .13, all $p > .05$) (Figure 8b). There were also no correlations between border score, HD modulation, or speed score (change in spatial correlation: $r$ ranged from −.15 to .09, all $p > .05$; change in rate overlap: $r$ ranged from −.10 to .03, all $p > .05$) (Figure 8c), suggesting that the subpopulation of non-grid cells that change over time does not correspond to a functional category of mEC cells. Thus, those cells that changed over time did not appear in any way distinct, nor would it have been possible to identify a priori which cells would change based on the activity pattern within a single session.

As we observed changes over time in both the spatial firing and overall firing rate of a subset of our non-grid cells we next sought to determine if there was any relation between the two modalities. Across all non-grid cells, there was a weak relationship between changes in space and changes in rate ($r = .38$, $p < .001$) with a few cells responding in both dimensions, but there were also a large number of cells that altered only their spatial pattern or only their firing rate (Figure 9a) suggesting that spatial firing patterns and overall firing rates are likely modulated independently. Lastly, as mEC superficial Layers 2 and 3 have highly differential projection patterns to CA3 and CA1 (van Strien et al., 2009), we asked if there were any anatomical

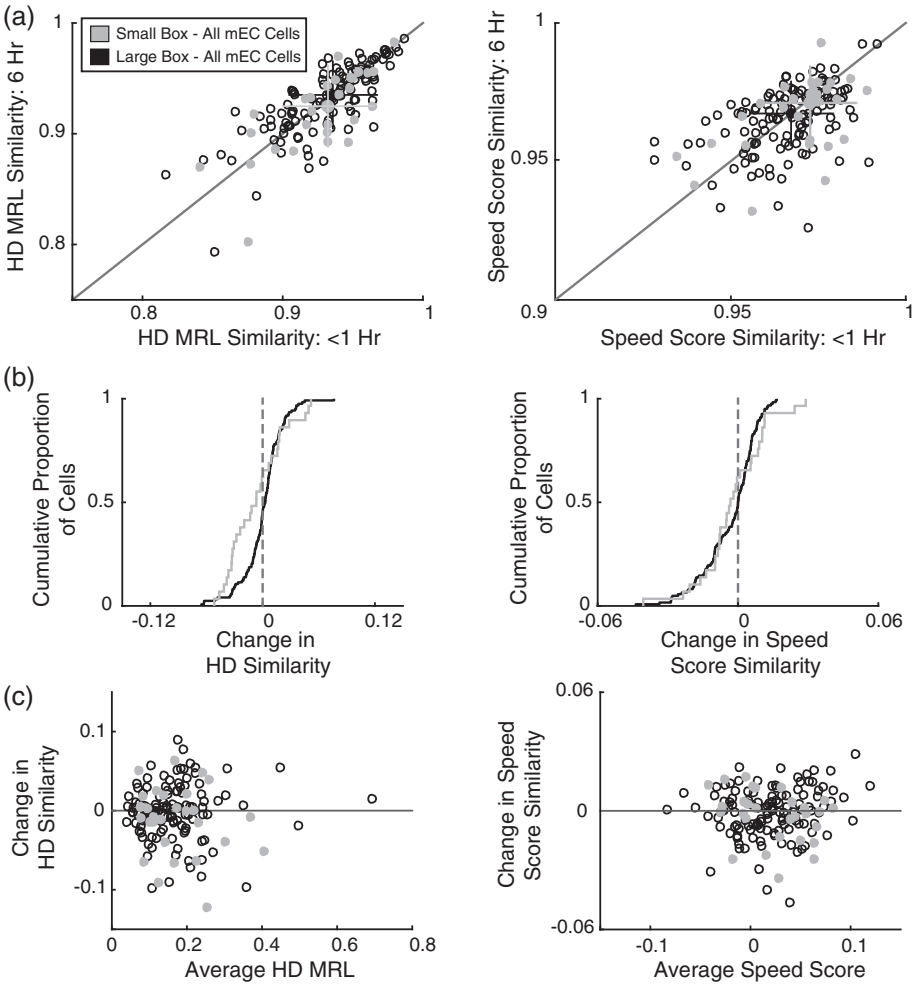


**FIGURE 7** Head direction and speed modulation did not vary systematically over a 6-hr period. (a, b) Similarity of HD modulation (left) and speed scores (right) of all mEC cells across sessions separated by less than 1 hr or 6 hrs are plotted as in Figure 4. Data for the two environment sizes are shown separately. (c) Change in HD modulation (left) and speed score similarity (right) across 6 hrs are plotted as a function of the cell's average across all recorded sessions

differences between non-grid cells that changed over time and those that did not. For both changes in spatial firing and changes in overall firing rate, we found on average no difference between non-grid cells recorded from Layer 2 and from Layer 3 (Layer 2 vs. Layer 3, change in spatial correlation: $z = 1.41$, $p > .05$; change in rate overlap: $z = -0.28$, $p > .05$). Yet, examination of the proportion of non-grid cells exhibiting significant changes in their spatial firing patterns over time revealed that these cells tended to be more abundant in mEC Layer 3 as compared to Layer 2 (proportion of Layer 2 vs. Layer 3 cells with significant change over time, spatial correlation: Chi-Sq = 5.88, $p < .05$; rate overlap: Chi-Sq = 0.10, $p > .05$) (Figure 9b). Thus, it appears that Layer 3 non-grid cells may be more likely to exhibit large scale changes in their spatial firing pattern over time, even though there was no clear difference between the average change of mEC Layer 2 compared to Layer 3 non-grid cells.

## 4 | DISCUSSION

Hippocampal spatial representations have previously been shown to change over time, and stability of hippocampal representations further decreases when inputs from mEC to hippocampus are damaged (Hales et al., 2014; Schlesiger et al., 2015). We therefore asked whether spatial firing patterns of mEC grid and non-grid cells are stable over extended time periods such that they are in a position to provide a stabilizing signal to the hippocampus. Within a single recording session, we found high precision and stability of spatial firing patterns for most mEC cells. However, environment size determined the degree of spatial precision. SI and WSC were significantly higher for both grid and irregular cells in a small box compared to a large box. Furthermore, while almost all irregular cells had spatial firing patterns above chance levels in the small box, about half of irregular cells were nonspatial in the large box. We then evaluated the consistency of mEC firing patterns over time. Irrespective of environment size, we observed that grid cell activity was highly consistent across repeated exposures to the same environment both over tens of minutes and over 6 hrs. Although the firing patterns of the collective non-grid cell population were less precise and stable than grid cells, changes in the activity patterns of the majority of the population were not correlated with elapsed time, with the exception of a subset of 10–20% of the population. In this small subset of non-grid cells, we observed a dramatic

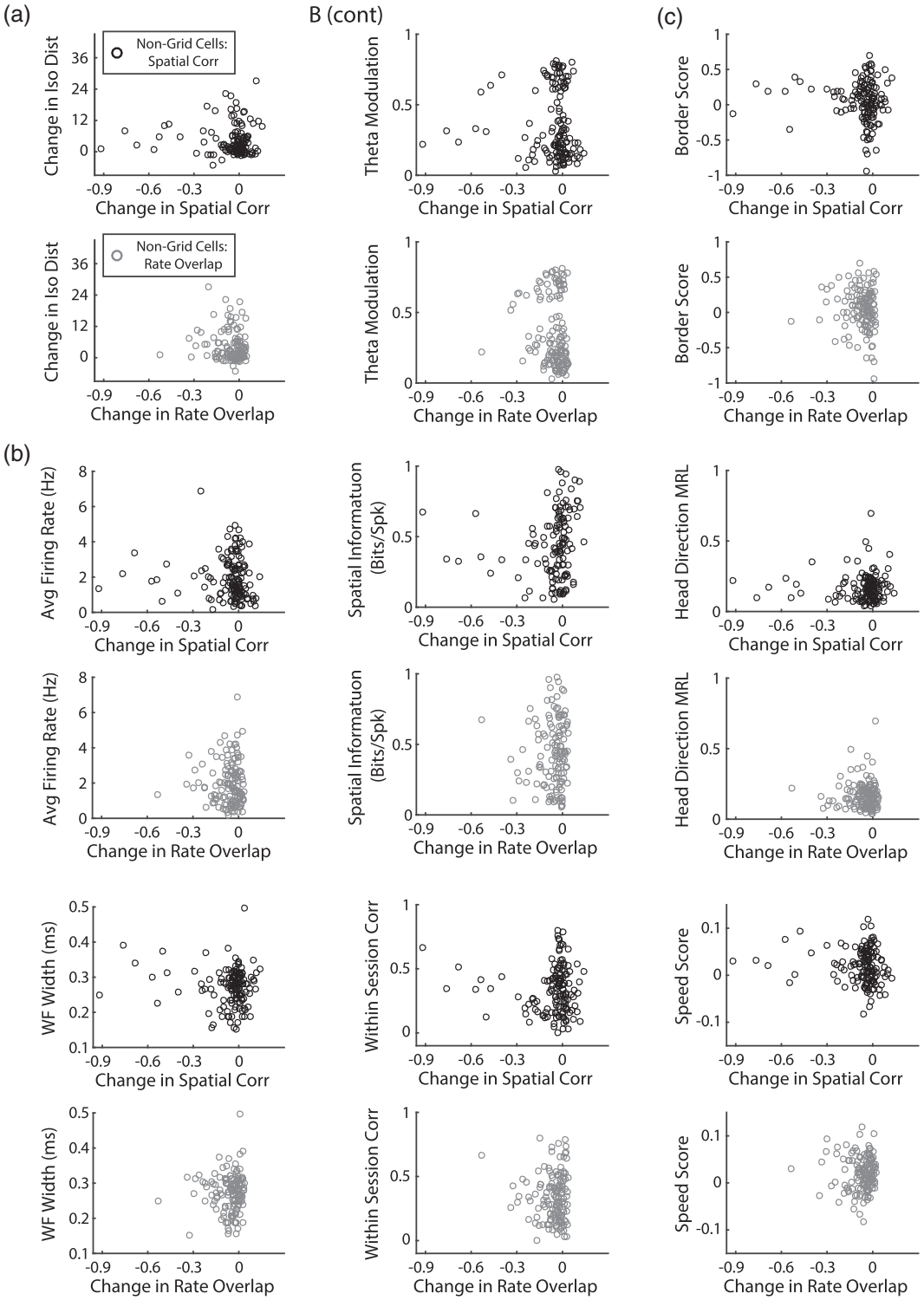


**FIGURE 8** Within the non-grid cell population there was no correspondence between changes in stability over time and other firing properties. (a) Changes in spatial correlation (top, black circles) and rate overlap (bottom, gray circles) over time were unrelated to changes in cluster isolation distance of mEC non-grid cells. (b) Changes over time were unrelated to various other characteristics of cell firing including average firing rate, waveform shape, theta modulation strength, SI, or WSC. (c) Changes in firing properties over time were unrelated to characteristics used to identify mEC cell classes of border cells, HD cells, and speed cells

change in the spatial firing or overall firing rate across a 6-hr period. Further investigation revealed that those non-grid cells that changed over time were preferentially recorded from Layer 3, but that we could not predict from the firing characteristics within a 10-min recording session whether a cell would show instability over longer time intervals. Taken together, our data suggest that the mEC grid cell input to hippocampus in conjunction with the majority of time invariant non-grid cells may aid in stabilizing hippocampal spatial maps, while a subset of time varying non-grid cells could provide complementary temporal information.

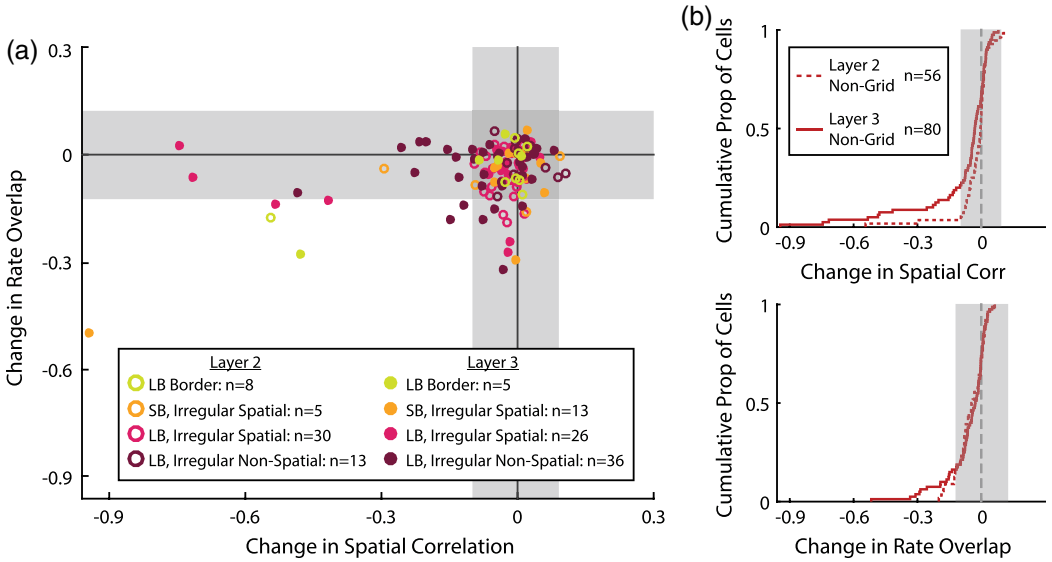


**FIGURE 9** Non-grid cells that changed over time were preferentially recorded from mEC Layer 3. (a) Comparison of the degree of change over time in spatial correlation and firing rate overlap of individual non-grid cells. Data are colored based on experimental paradigm and cell class. Irregular cells recorded in the large environment are further divided into spatial and nonspatial cells. Cells are also categorized based on their putative anatomical location within mEC Layer 2 or Layer 3. Chance distributions for spatial correlation and rate overlap are shown as shaded regions, redrawn from Figure 4d. (b) Changes in spatial correlation (top) and firing rate overlap (bottom) are presented separately for non-grid cells recorded from Layer 2 and Layer 3. LB, large box. SB, small box [Color figure can be viewed at wileyonlinelibrary.com]

Many previous studies have identified a substantial subset of mEC cells as nonspatial (Kropff et al., 2015; Latuske et al., 2015; Tang et al., 2014; Tang et al., 2015; Zhang et al., 2013). In contrast, recent work utilizing more sophisticated classification criteria found that almost all mEC cells exhibit some degree of spatial firing (Diehl et al., 2017; Hardcastle, Maheswaranathan, et al., 2017b). Our data add to these findings with two main results. First, our finding that SI and WSC, two metrics for evaluating spatial firing patterns, are both unimodally distributed suggests that spatial firing of mEC cells would be more appropriately described as a continuum, as opposed to discrete classes of spatial and nonspatial cells. For example, we observed some degree of spatial stability even in nonspatial irregular cells and no differences in the stability of spatial firing properties over time in irregular cells irrespective of whether they were classified as spatial or nonspatial. These findings are consistent with the interpretation that spatial and nonspatial cells are not mEC cell types that can be unambiguously separated. Second, we observed significantly higher SI and WSC values for cells recorded in a smaller compared to a larger box. The size of an environment thus has a substantial impact on the spatial firing properties of mEC cells. Theoretical work has proposed that spatial firing in mEC and hippocampus is strongly influenced by interactions with environmental boundaries or other highly salient spatial landmarks (Barry et al., 2006; Fuhs and Touretzky, 2006; Gothard et al., 1996; Hartley et al., 2000), such that larger environments with more distant boundaries would be predicted to result in poorer spatial representations. Such an idea has gained experimental support by the finding that hippocampal place fields are reliably generated in novel small environments but not in larger ones following pharmacological inactivation of the medial septal area. (Brandon et al., 2014; Wang et al., 2015). Additionally, fine scale analysis of grid cell firing revealed a gradual accumulation of error in spiking location that was corrected after interactions with a border region (Hardcastle et al., 2015). Larger environments with more distant borders would thus be predicted to lead to greater error accumulation in spatial spiking. Accordingly, we found that the spatial firing of mEC grid and non-grid cells is influenced by environment size.

Along with identifying an effect of environment size on spatial firing of both grid and irregular cells, we found that grid, border, and irregular cells all varied their firing patterns as a function of time to a similar degree over periods of less than 1 hr. While the spatial correlation between sessions was high in grid cells and low in irregular cells, it remained consistent over extended time intervals for each mEC cell type and for individual cells, such that is was at approximately the same level across 15, 30, and 45 min, even for cells with low average spatial similarity. Furthermore, the spatial correlation of even the least spatial mEC cells did not reach chance levels, indicating that the similarity across sessions had not reached a floor, and that similarity could theoretically decrease over time. Thus, the majority of mEC firing patterns did not simply drift randomly over time, with increasing time leading to progressively more drift, but rather varied around a stable set point, with grid cells exhibiting less variation around this point and irregular cells exhibiting more. In comparing to hippocampal place cells, the majority of mEC cells thus resemble the behavior of CA3 over tens of minutes. While the baseline reliability of CA3 place cells is considerably higher than most mEC cells (see low spatial correlation values for mEC non-grid cells in Figures 3b and 4c), both regions exhibit temporally stable firing patterns with no relative decrease in similarity from the respective baselines. This serves in stark contrast to the CA2 region where, even though baseline reliability is generally high, systematic changes over time are already evident over tens of minutes (Mankin et al., 2015).

Major differences in the stability over time of grid cells compared to non-grid cells began to emerge when examining spatial firing

patterns over periods of 6 hrs. Consistent with the notion that grid cells may provide a universal spatial signal (Moser et al., 2008; Moser et al., 2014), the stability of the grid signal remained high over extended time periods. While changes in firing patterns over time were also not observed in many non-grid cells, the non-grid population was distinct in that it also included a subset of cells that changed. These observations suggest that a subpopulation of mEC non-grid cells may convey temporal information. Conversely, grid cells and the large proportion of relatively stable non-grid cells may be a key source of inputs to stabilize hippocampal maps.

One possibility that arises is that the subpopulation of mEC non-grid cells that changed over time reflected a distinct functional cell type, perhaps one dedicated to temporal coding. However, owing to the fact that we saw no clear separation or indication of bimodality in our distributions of change over time (Figure 4d and 9a) and the lack of clear correspondence to any other firing properties, our data do not support such a conclusion. Perhaps instead, systematic change over time should not be thought of as falling into discrete categories but rather that cells sit at various points on a continuum, perhaps not unlike other functional properties in which mEC appears to be a strongly heterogeneous population (Hardcastle, Ganguli, et al., 2017a).

Yet, stability or change over time does not appear to be uniform across the mEC. The difference in the degree of variability over time between Layer 2 and Layer 3 cells may reflect an important relationship to hippocampal coding, with the more stable Layer 2 population projecting to CA3 in support of a more stable representation and the more time varying Layer 3 population projecting to CA1 in contribution to a more time varying representation (Mankin et al., 2012; van Strien et al., 2009). As CA2 receives input from both mEC Layer 2 and Layer 3 (Chevaleyre and Siegelbaum, 2010; Cui et al., 2013; Hitti and Siegelbaum, 2014; but see Kohara et al., 2014), a time varying signal could be inherited from the small subpopulation of highly varying mEC cells, although given the large proportion of CA2 cells that change over time and the large degree to which the network changes (Lu et al., 2015; Mankin et al., 2015) other inputs or local integration within the CA2 region are also likely sources of variability over time.

However, it must also be recognized that not all mEC Layer 3 cells altered their firing properties over time, and that not all mEC cells, either in Layer 2 or Layer 3, project directly to hippocampus (Tang et al., 2015; Varga et al., 2010; Zhang et al., 2013). An equally feasible situation then is that those non-grid cells which changed over time could project exclusively within mEC, or that the mEC projection downstream to hippocampus is composed of a mixed population of cells that change over time and cells that do not change. While attempts have been made to associate the in vivo firing patterns, genetic and morphological profiles, and anatomical connections of individual mEC cells (Latuske et al., 2015; Sun et al., 2015; Tang et al., 2014; Zhang et al., 2013), there has been limited success in linking different classes of mEC cells and determining a clear, comprehensive wiring diagram of entorhinal-hippocampal interactions. Future studies and new methods are thus required to establish a more direct relation between the inputs to hippocampus and the time-varying firing patterns across hippocampal subregions.

Here, we find that mEC provides hippocampus with a diverse set of spatially selective inputs of which most are highly stable over time, a necessary feature for establishing reliable spatial maps. Yet hippocampus complements its spatial representation with information about elapsed time, a feature that we also observe in only a subset of mEC non-grid cells. Thus, our data suggest a possible contribution of mEC to the diversity of temporal coding and the possibility that CA1 and CA2 inherit a time varying signal from mEC Layer 3 non-grid cells. Importantly, we also find that the majority of the medial entorhinal projection is highly reliable across time, consistent with findings from lesion studies indicating a major role of mEC in providing hippocampus with a stable spatial code over minutes and hours (Hales et al., 2014; Schlesiger et al., 2015).

## ACKNOWLEDGMENTS

We thank B. Boublil, A.-L. Schlenner, and M. Wong for technical assistance. Research was supported by National Institute of Health grants MH-100349, MH-102841, the Whitehall Foundation 20130571, and a Walter F. Heiligenberg Professorship to J.K.L, and National Institute of Health grants NS-097772, NS-084324, and NS-086947 to S.L. The authors declare no competing financial interests.

## AUTHOR CONTRIBUTIONS

G.W.D., S.L. and J.K.L. designed research, G.W.D. and O.J.H. collected data, G.W.D. analyzed data, and G.W.D., S.L., and J.K.L. wrote the manuscript.

## ORCID

*Jill K. Leutgeb* http://orcid.org/0000-0002-2014-842X

## REFERENCES

Barry, C., Lever, C., Hayman, R., Hartley, T., Burton, S., O'Keefe, J., … Burgess, N. (2006). The boundary vector cell model of place cell firing and spatial memory. *Reviews in the Neurosciences*, *17*(1–2), 71–97.

Blair, H. T., Gupta., K., & Zhang, K. (2008). Conversion of a phase- to a rate-coded position signal by a three-stage model of theta cells, grid cells, and place cells. *Hippocampus*, *18*(12), 1239–1255.

Brandon, M. P., Koenig, J., Leutgeb, J. K., & Leutgeb, S. (2014). New and distinct hippocampal place codes are generated in a new environment during septal inactivation. *Neuron*, *82*(4), 789–796.

Brun, V. H., Leutgeb, S., Wu, H. Q., Schwarcz, R., Witter, M. P., Moser, E. I., & Moser, M. B. (2008). Impaired spatial representation in CA1 after lesion of direct input from entorhinal cortex. *Neuron*, *57*(2), 290–302.

Buzsaki, G., & Moser, E. I. (2013). Memory, navigation and theta rhythm in the hippocampal-entorhinal system. *Nature Neuroscience*, *16*(2), 130–138.

Cheng, S., & Frank, L. M. (2011). The structure of networks that produce the transformation from grid cells to place cells. *Neuroscience*, *197*, 293–306.

Chevaleyre, V., & Siegelbaum, S. A. (2010). Strong CA2 pyramidal neuron synapses define a powerful disynaptic cortico-hippocampal loop. *Neuron*, *66*(4), 560–572.

Cui, Z., Gerfen, C. R., & Young, W. S., III. (2013). Hypothalamic and other connections with dorsal CA2 area of the mouse hippocampus. *The Journal of Comparative Neurology*, *521*(8), 1844–1866.

de Almeida, L., Idiart, M., & Lisman, J. E. (2009). The input-output transformation of the hippocampal granule cells: From grid cells to place fields. *The Journal of Neuroscience*, *29*(23), 7504–7512.

Diehl, G. W., Hon, O. J., Leutgeb, S., & Leutgeb, J. K. (2017). Grid and non-grid cells in medial Entorhinal cortex represent spatial location and environmental features with complementary coding schemes. *Neuron*, *94*(1), 83–92e6.

Dudek, S. M., Alexander, G. M., & Farris, S. (2016). Rediscovering area CA2: Unique properties and functions. *Nature Reviews. Neuroscience*, *17*(2), 89–102.

Estes, W. K. (1955). Statistical theory of spontaneous recovery and regression. *Psychological Review*, *62*(3), 145–154.

Ezzyat, Y., & Davachi, L. (2014). Similarity breeds proximity: Pattern similarity within and across contexts is related to later mnemonic judgments of temporal proximity. *Neuron*, *81*(5), 1179–1189.

Fuhs, M. C., & Touretzky, D. S. (2006). A spin glass model of path integration in rat medial entorhinal cortex. *The Journal of Neuroscience*, *26*(16), 4266–4276.

Fyhn, M., Molden, S., Witter, M. P., Moser, E. I., & Moser, M. B. (2004). Spatial representation in the entorhinal cortex. *Science*, *305*(5688), 1258–1264.

Gothard, K. M., Skaggs, W. E., Moore, K. M., & McNaughton, B. L. (1996). Binding of hippocampal CA1 neural activity to multiple reference frames in a landmark-based navigation task. *The Journal of Neuroscience*, *16*(2), 823–835.

Hafting, T., Fyhn, M., Molden, S., Moser, M. B., & Moser, E. I. (2005). Microstructure of a spatial map in the entorhinal cortex. *Nature*, *436*(7052), 801–806.

Hales, J. B., Schlesiger, M. I., Leutgeb, J. K., Squire, L. R., Leutgeb, S., & Clark, R. E. (2014). Medial entorhinal cortex lesions only partially disrupt hippocampal place cells and hippocampus-dependent place memory. *Cell Reports*, *9*(3), 893–901.

Hardcastle, K., Ganguli, S., & Giocomo, L. M. (2015). Environmental boundaries as an error correction mechanism for grid cells. *Neuron*, *86*(3), 827–839.

Hardcastle, K., Ganguli, S., & Giocomo, L. M. (2017a). Cell types for our sense of location: Where we are and where we are going. *Nature Neuroscience*, *20*(11), 1474–1482.

Hardcastle, K., Maheswaranathan, N., Ganguli, S., & Giocomo, L. M. (2017b). A multiplexed, heterogeneous, and adaptive code for navigation in medial Entorhinal cortex. *Neuron*, *94*(2), 375–387e7.

Hartley, T., Burgess, N., Lever, C., Cacucci, F., & O'Keefe, J. (2000). Modeling place fields in terms of the cortical inputs to the hippocampus. *Hippocampus*, *10*(4), 369–379.

Hartley, T., Lever, C., Burgess, N., & O'Keefe, J. (2014). Space in the brain: How the hippocampal formation supports spatial cognition. *Philosophical Transactions of the Royal Society of London. Series B, Biological Sciences*, *369*(1635), 20120510.

Hitti, F. L., & Siegelbaum, S. A. (2014). The hippocampal CA2 region is essential for social memory. *Nature*, *508*(7494), 88–92.

Howard, M. W., & Kahana, M. J. (2002). A distributed representation of temporal context. *Journal of Mathematical Psychology*, *46*(3), 269–299.

Hsieh, L. T., Gruber, M. J., Jenkins, L. J., & Ranganath, C. (2014). Hippocampal activity patterns carry information about objects in temporal context. *Neuron*, *81*(5), 1165–1178.

Jenkins, L. J., & Ranganath, C. (2016). Distinct neural mechanisms for remembering when an event occurred. *Hippocampus*, *26*(5), 554–559.

Jones, M. W., & McHugh, T. J. (2011). Updating hippocampal representations: CA2 joins the circuit. *Trends in Neurosciences*, *34*(10), 526–535.

Kohara, K., Pignatelli, M., Rivest, A. J., Jung, H. Y., Kitamura, T., Suh, J., … Tonegawa, S. (2014). Cell type-specific genetic and optogenetic tools reveal hippocampal CA2 circuits. *Nature Neuroscience*, *17*(2), 269–279.

Kropff, E., Carmichael, J. E., Moser, M. B., & Moser, E. I. (2015). Speed cells in the medial entorhinal cortex. *Nature*, *523*(7561), 419–424.

Latuske, P., Toader, O., & Allen, K. (2015). Interspike intervals reveal functionally distinct cell populations in the medial Entorhinal cortex. *The Journal of Neuroscience*, *35*(31), 10963–10976.

Lu, L., Igarashi, K. M., Witter, M. P., Moser, E. I., & Moser, M. B. (2015). Topography of place maps along the CA3-to-CA2 Axis of the hippocampus. *Neuron*, *87*(5), 1078–1092.

Mankin, E. A., Diehl, G. W., Sparks, F. T., Leutgeb, S., & Leutgeb, J. K. (2015). Hippocampal CA2 activity patterns change over time to a larger extent than between spatial contexts. *Neuron*, *85*(1), 190–201.

Mankin, E. A., Sparks, F. T., Slayyeh, B., Sutherland, R. J., Leutgeb, S., & Leutgeb, J. K. (2012). Neuronal code for extended time in the hippocampus. *Proceedings of the National Academy of Sciences of the United States of America*, *109*(47), 19462–19467.

Manning, J. R., Polyn, S. M., Baltuch, G. H., Litt, B., & Kahana, M. J. (2011). Oscillatory patterns in temporal lobe reveal context reinstatement during memory search. *Proceedings of the National Academy of Sciences of the United States of America*, *108*(31), 12893–12897.

Miao, C., Cao, Q., Ito, H. T., Yamahachi, H., Witter, M. P., Moser, M. B., & Moser, E. I. (2015). Hippocampal remapping after partial inactivation of the medial Entorhinal cortex. *Neuron*, *88*(3), 590–603.

Moser, E. I., Kropff, E., & Moser, M. B. (2008). Place cells, grid cells, and the brain's spatial representation system. *Annual Review of Neuroscience*, *31*, 69–89.

Moser, E. I., Roudi, Y., Witter, M. P., Kentros, C., Bonhoeffer, T., & Moser, M. B. (2014). Grid cells and cortical representation. *Nature Reviews. Neuroscience*, *15*(7), 466–481.

Newman, E. L., & Hasselmo, M. E. (2014). Grid cell firing properties vary as a function of theta phase locking preferences in the rat medial entorhinal cortex. *Frontiers in Systems Neuroscience*, *8*, 193.

Nielson, D. M., Smith, T. A., Sreekumar, V., Dennis, S., & Sederberg, P. B. (2015). Human hippocampus represents space and time during retrieval of real-world memories. *Proceedings of the National Academy of Sciences of the United States of America*, *112*(35), 11078–11083.

O'Keefe, J., & Burgess, N. (1996). Geometric determinants of the place fields of hippocampal neurons. *Nature*, *381*(6581), 425–428.

Ormond, J., & McNaughton, B. L. (2015). Place field expansion after focal MEC inactivations is consistent with loss of Fourier components and path integrator gain reduction. *Proceedings of the National Academy of Sciences of the United States of America*, *112*(13), 4116–4121.

Perez-Escobar, J. A., Kornienko, O., Latuske, P., Kohler, L., & Allen, K. (2016). Visual landmarks sharpen grid cell metric and confer context specificity to neurons of the medial entorhinal cortex. *eLife*, *5*, e16937.

Robinson, N. T. M., Priestley, J. B., Rueckemann, J. W., Garcia, A. D., Smeglin, V. A., Marino, F. A., & Eichenbaum, H. (2017). Medial Entorhinal cortex selectively supports temporal coding by hippocampal neurons. *Neuron*, *94*(3), 677–688.e6.

Rolls, E. T., Stringer, S. M., & Elliot, T. (2006). Entorhinal cortex grid cells can map to hippocampal place cells by competitive learning. *Network*, *17*(4), 447–465.

Rubin, A., Geva, N., Sheintuch, L., & Ziv, Y. 2015. Hippocampal ensemble dynamics timestamp events in long-term memory. *eLife*, *4*, e12247.

Rueckemann, J. W., DiMauro, A. J., Rangel, L. M., Han, X., Boyden, E. S., & Eichenbaum, H. (2016). Transient optogenetic inactivation of the medial entorhinal cortex biases the active population of hippocampal neurons. *Hippocampus*, *26*(2), 246–260.

Sargolini, F., Fyhn, M., Hafting, T., McNaughton, B. L., Witter, M. P., Moser, M. B., & Moser, E. I. (2006). Conjunctive representation of position, direction, and velocity in entorhinal cortex. *Science*, *312*(5774), 758–762.

Savelli, F., Yoganarasimha, D., & Knierim, J. J. (2008). Influence of boundary removal on the spatial representations of the medial entorhinal cortex. *Hippocampus*, *18*(12), 1270–1282.

Schlesiger, M. I., Cannova, C. C., Boublil, B. L., Hales, J. B., Mankin, E. A., Brandon, M. P., … Leutgeb, S. (2015). The medial entorhinal cortex is necessary for temporal organization of hippocampal neuronal activity. *Nature Neuroscience*, *18*(8), 1123–1132.

Schmitzer-Torbert, N., Jackson, J., Henze, D., Harris, K., & Redish, A. D. (2005). Quantitative measures of cluster quality for use in extracellular recordings. *Neuroscience*, *131*(1), 1–11.

Skaggs, W. E., McNaughton, B. L., Gothard, K. M., & Markus, E. J. (1993). An information-theoretic approach to deciphering the hippocampal code. *Advances in Neural Information Processing Systems*, *5*, 1030–1037.

Skillings, J. H., & Mack, G. A. (1981). On the use of a Friedman-type statistic in balanced and un-balanced block-designs. *Technometrics*, *23*(2), 171–177.

Solstad, T., Boccara, C. N., Kropff, E., Moser, M. B., & Moser, E. I. (2008). Representation of geometric borders in the entorhinal cortex. *Science*, *322*(5909), 1865–1868.

Solstad, T., Moser, E. I., & Einevoll, G. T. (2006). From grid cells to place cells: A mathematical model. *Hippocampus*, *16*(12), 1026–1031.

Sun, C., Kitamura, T., Yamamoto, J., Martin, J., Pignatelli, M., Kitch, L. J., … Tonegawa, S. (2015). Distinct speed dependence of entorhinal island and ocean cells, including respective grid cells. *Proceedings of the National Academy of Sciences of the United States of America*, *112*(30), 9466–9471.

Tang, Q., Burgalossi, A., Ebbesen, C. L., Ray, S., Naumann, R., Schmidt, H., … Brecht, M. (2014). Pyramidal and stellate cell specificity of grid and border representations in layer 2 of medial entorhinal cortex. *Neuron*, *84*(6), 1191–1197.

Tang, Q., Ebbesen, C. L., Sanguinetti-Scheck, J. I., Preston-Ferrer, P., Gundlfinger, A., Winterer, J., … Burgalossi, A. (2015). Anatomical organization and spatiotemporal firing patterns of layer 3 neurons in the rat medial Entorhinal cortex. *The Journal of Neuroscience*, *35*(36), 12346–12354.

Thompson, L. T., & Best, P. J. (1989). Place cells and silent cells in the hippocampus of freely-behaving rats. *The Journal of Neuroscience*, *9*(7), 2382–2390.

Tulving, E. (1972). *Episodic and semantic memory. Organization of memory (p xiii, 423-xiii, 423)*. Oxford, England: Academic Press.

van Strien, N. M., Cappaert, N. L., & Witter, M. P. (2009). The anatomy of memory: An interactive overview of the parahippocampal-hippocampal network. *Nature Reviews. Neuroscience*, *10*(4), 272–282.

Varga, C., Lee, S. Y., & Soltesz, I. (2010). Target-selective GABAergic control of entorhinal cortex output. *Nature Neuroscience*, *13*(7), 822–824.

Wang, Y., Romani, S., Lustig, B., Leonardo, A., & Pastalkova, E. (2015). Theta sequences are essential for internally generated hippocampal firing fields. *Nature Neuroscience*, *18*(2), 282–288.

Zhang, S. J., Ye, J., Miao, C., Tsao, A., Cerniauskas, I., Ledergerber, D., … Moser, E. I. (2013). Optogenetic dissection of entorhinal-hippocampal functional connectivity. *Science*, *340*(6128), 1232627.

Ziv, Y., Burns, L. D., Cocker, E. D., Hamel, E. O., Ghosh, K. K., Kitch, L. J., … Schnitzer, M. J. (2013). Long-term dynamics of CA1 hippocampal place codes. *Nature Neuroscience*, *16*(3), 264–266.

**How to cite this article:** Diehl GW, Hon OJ, Leutgeb S, Leutgeb JK. Stability of medial entorhinal cortex representations over time. *Hippocampus*. 2018;1–19. https://doi.org/10.1002/hipo.23017